POLITECNICO MILANO 1863

SCUOLA DI INGEGNERIA INDUSTRIALE E DELL'INFORMAZIONE

Comparative Analysis of 400 V AC and Bipolar 800 V DC Power Distribution Architectures for a Hyperscale Data Center

TESI DI LAUREA MAGISTRALE IN
ELECTRICAL ENGINEERING
INGEGNERIA ELETTRICA

Author: **Shakiba Rahmatijami Mahmoudabadi**

Student ID: 10949595
Advisor: Prof. Morris Brenna
Co-advisor: Osama Elhassan
Academic Year: 2025-26

Abstract

Keywords: data center, DC distribution, copper usage, power losses, reliability, and availability

This thesis investigates the potential benefits of adopting bipolar 800 V DC (± 400 V) power-distribution architecture in large-scale data centers, compared to a conventional low voltage AC solution. With the rapid growth of data center capacity, power efficiency, material usage, and system reliability have become critical design challenges, particularly at the distribution level.

A comparative analysis is carried out between existing 400 V AC architecture and proposed DC architecture under consistent routing, load distribution, and redundancy assumptions. The study focuses on three main aspects: conductor sizing and copper usage, electrical distribution losses, and system availability and reliability. Conductor sizing is evaluated across multiple distribution levels to quantify copper mass and cable cost implications. Electrical losses are analyzed using one year of measured operational data to estimate annual energy losses. System availability is assessed using a reliability block diagram approach based on standardized component reliability data.

The results show that the higher operating voltage of the DC architecture significantly reduces current levels, enabling smaller conductor cross-sections and a substantial reduction in total copper usage. Distribution losses are also reduced due to lower current-related losses and the elimination of inverter stages in the power path. From the reliability perspective, the DC architecture exhibits improved availability and reliability at both system and load levels, driven by a simplified conversion chain and a reduced number of critical components.

Overall, the findings demonstrate that bipolar 800 V DC distribution represents a technically viable and advantageous alternative to conventional AC architectures for large-scale data centers, with potential benefits in efficiency, material usage, and reliability.

Abstract in Italiano

Questa tesi analizza i potenziali vantaggi dell'adozione di un'architettura di distribuzione dell'energia in corrente continua bipolare a 800 V (±400 V) nei data center di grande scala, rispetto a una soluzione tradizionale in bassa tensione in corrente alternata. Con la rapida crescita della capacità dei data center, l'efficienza energetica, l'utilizzo dei materiali e l'affidabilità del sistema sono diventati aspetti critici di progetto, in particolare a livello di distribuzione.

Viene condotta un'analisi comparativa tra un'architettura AC esistente a 400 V e la proposta architettura DC, assumendo ipotesi coerenti su instradamento, distribuzione dei carichi e criteri di ridondanza. Lo studio si concentra su tre aspetti principali: il dimensionamento dei conduttori e l'utilizzo del rame, le perdite di distribuzione elettrica e la disponibilità e affidabilità del sistema. Il dimensionamento dei conduttori è valutato su più livelli di distribuzione al fine di quantificare la massa di rame e le implicazioni economiche dei cavi. Le perdite elettriche sono analizzate utilizzando un anno di dati operativi misurati per stimare le perdite energetiche annuali. La disponibilità del sistema è valutata mediante un approccio basato su diagrammi a blocchi di affidabilità, utilizzando dati di affidabilità standardizzati dei componenti.

I risultati mostrano che la maggiore tensione di esercizio dell'architettura DC riduce significativamente i livelli di corrente, consentendo l'adozione di sezioni di conduttori inferiori e una sostanziale riduzione dell'utilizzo complessivo di rame. Le perdite di distribuzione risultano inoltre ridotte grazie alla diminuzione delle perdite legate alla corrente e all'eliminazione degli stadi di conversione a inverter nel percorso di alimentazione. Dal punto di vista dell'affidabilità, l'architettura DC presenta una disponibilità superiore sia a livello di sistema sia a livello di carico, grazie a una catena di conversione semplificata e a un numero ridotto di componenti critici.

Nel complesso, i risultati dimostrano che la distribuzione in corrente continua bipolare a 800 V rappresenta un'alternativa tecnicamente valida e vantaggiosa rispetto alle architetture AC convenzionali per i data center di grande scala, offrendo potenziali benefici in termini di efficienza, utilizzo dei materiali e affidabilità.

Contents

1 Introduction

1.1. Motivation and Background

Data centers form the modern digital infrastructure by supporting cloud computing, large-scale data storage, and high availability network services. Their rapid global expansion has led to a continuous increase in installed electrical capacity, making power efficiency, reliability, and material usage key design constraints. In large facilities, even small improvements in power-distribution efficiency or component reduction can result in significant savings in operating costs and environmental impacts over the system lifetime.

Low voltage AC distribution has traditionally been adopted in data centers due to its direct compatibility with the utility grid and the widespread availability of standardized equipment. However, most internal data center loads, including servers, storage devices, and network equipment, ultimately operate on DC. Energy storage systems and on-site renewable sources are also inherently DC-based. Consequently, conventional AC architecture requires multiple power-conversion stages, which increase electrical losses, system complexity, and overall availability.

In response to these limitations, DC distribution architecture has gained renewed interest, particularly for large-scale and high power-density data centers. Efficiency assessment approaches in LVAC/LVDC literatures emphasize that converter losses can represent a dominant share of total losses in AC architectures, and that DC distribution can reduce the power loss by reducing downstream conversion stages; Figure 1 shows the hourly power loss in a month in the case-study evaluated by Jiang *et al*. [1], showing around 40% lower power loss for DC. Additionally, by increasing the DC voltage level, which leads to reduction in current levels, followed by eliminating conversion stages, and simplifying power paths, DC systems can offer significant advantages also in terms of conductor sizing, copper usage, and reliability.

Among the proposed solutions, bipolar DC architectures operating at ± 400 V (800 V DC) are especially attractive, as they combine reduced current with improved fault tolerance, compatibility with existing insulation practices, and capability of feeding both 800 V and 400 V loads.

This thesis presents a comparative analysis of existing AC power-distribution architecture and proposed bipolar 800 V DC architecture for a large-scale data center. The comparison focuses on three main aspects: (I) conductor sizing and copper usage,

(II) distribution losses and their annual energy impact using measured operational data, and (III) system availability and reliability evaluated through reliability block diagram modeling. To ensure consistency, both architectures are analyzed under identical routing, load distribution, and redundancy assumptions.

A high-level overview of the AC and DC architectures considered in this study is presented in the following subsection to define the system boundary and the main functional blocks. Chapter 2 is an article review, generally explaining the features of data centers, their limitations, and improvement scenarios. Detailed sizing procedures, copper calculations, and economic assumptions are developed in Chapter 3, while electrical losses and reliability analyses are addressed in Chapter 4 and Chapter 5, respectively.

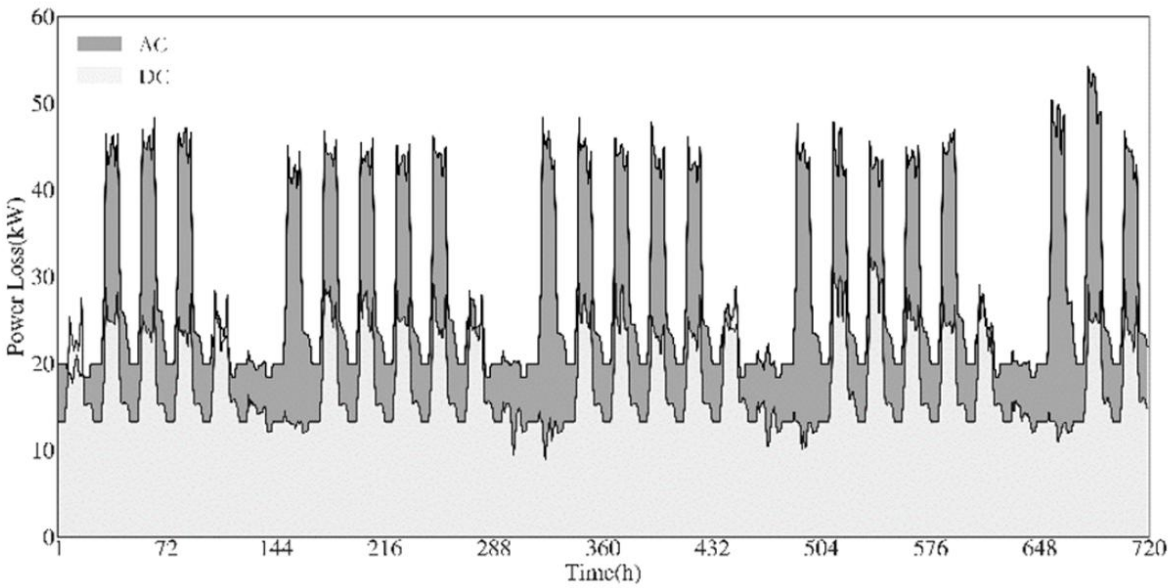

Figure 1. Hourly power loss for AC and DC in a month

1.2. System Architecture

A simplified flowchart of the existing AC system and the proposed DC system in this study is shown in Figure 2.

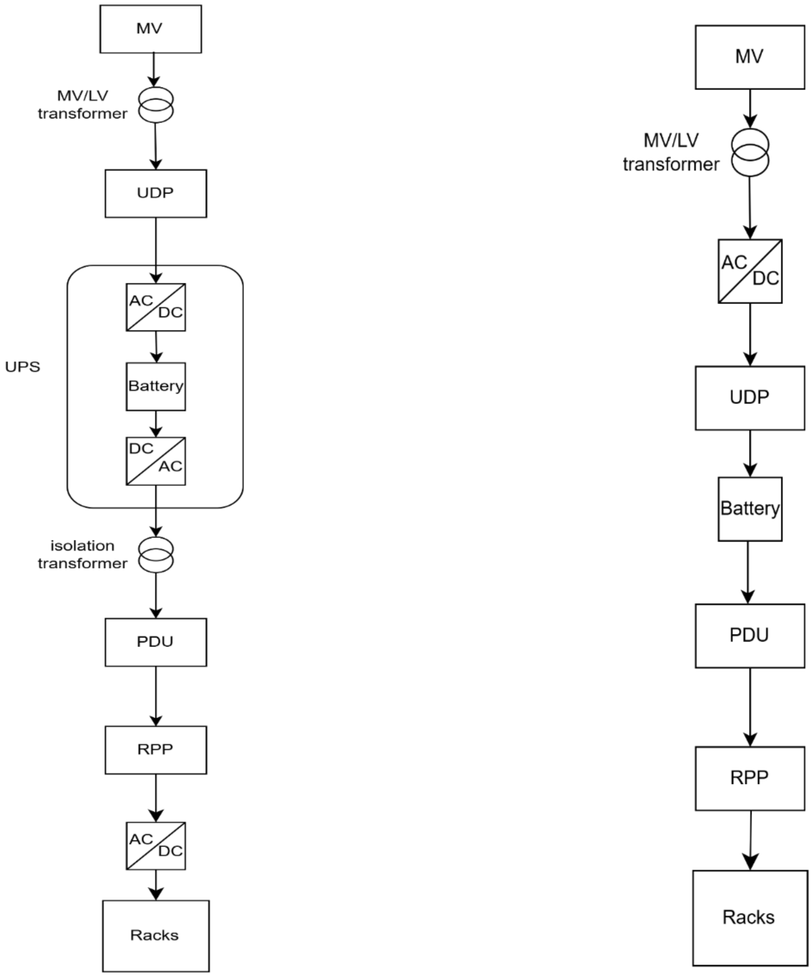

(a) Current AC configuration (b) Proposed DC configuration

Figure 2. Simplified flowchart of the AC and DC architectures under study.

The architecture shown is intended to define the system boundary and modeling assumptions. Each level (UDP, PDU, RPP) represents a distribution bus serving as a common electrical node for multiple downstream loads. As illustrated in Figure 2, the DC configuration differs from the AC model in the following key aspects:

1. The AC UPS system is replaced by a DC battery system.
2. The isolation transformer is eliminated in the DC system, as isolation is already provided upstream at the MV/LV transformer.

3. The AC/DC converter previously located at the load side is shifted upstream, immediately after the MV/LV transformer, instead of being installed locally at each load.

Collectively, because the final load uses DC for operation, these modifications reduce the number of power-conversion stages, improve end-to-end efficiency and system reliability, while also simplifying the overall power distribution architecture. Additionally, eliminating the isolation transformer and the inverter, together with a lower number of rectifiers (from one rectifier per load to one per battery system) can potentially reduce Cap-Ex.

2 Article Review

This section reviews scientific and technical literature related to this work, with particular emphasis on data centers. The objective is to provide the background necessary to understand the role of data centers, their growing importance, and the key challenges associated with their energy consumption and reliability. The reviewed works are organized to support a clear and structured discussion.

The section first introduces the concept of a data center and outlines its fundamental components and functions. It then discusses the increasing importance of data centers and their rapid growth in recent years, driven by the expansion of digital services. Subsequently, recent improvements and emerging technologies in data center design are reviewed. Finally, the literature comparing AC and DC power distribution architectures is examined to motivate the analysis presented in the following chapters.

2.1. What Is a Data Center and Why Is It Important?

A data center is a dedicated facility designed to host, operate, and protect Information Technology (IT) equipment such as servers, storage systems, and networking devices, together with the supporting infrastructure required to ensure their continuous and reliable operation. This supporting infrastructure typically includes electrical power supply systems, power distribution and protection equipment, cooling and ventilation systems, monitoring and control platforms, and physical security measures. The primary objective of a data center is to provide a controlled environment in which digital services can be delivered with high availability, performance, and data integrity [2], [3].

From a functional perspective, data centers can be described as complex cyber-physical systems in which IT loads and infrastructure loads are tightly coupled. While servers and networking equipment perform computation, storage, and data transmission, the power and cooling systems ensure that these operations can be sustained under varying load conditions and fault scenarios. As highlighted by Shehabi et al., the total energy consumption of a data center is not limited to the IT equipment itself but also includes significant overhead associated with power conversion, distribution losses, cooling system, and auxiliary services [4]. This interaction between digital workloads and physical infrastructure is one of the defining characteristics of modern data centers and is crucial for their design and optimization.

Data centers form the backbone of today's digital economy; cloud computing platforms, enterprise information systems, financial services, social networks, scientific computing, and increasingly Artificial Intelligence (AI) applications all rely on data center infrastructure. As a result, the reliability and efficiency of data centers have become critical not only from a technical standpoint but also from an economic and societal perspective. Even short service interruptions can lead to financial losses and operational disruptions, which explains why data center design traditionally prioritizes redundancy, fault tolerance, and high availability over energy efficiency considerations [5].

On the other hand, the growing importance of data centers is reflected in their energy footprint. Large-scale studies conducted at national and global levels show that data centers represent a non-negligible share of electricity consumption, particularly in highly digitalized economies [4], [6]. Although continuous improvements in server efficiency and virtualization have partially mitigated energy growth, the absolute demand for digital services continues to increase. Consequently, data centers are now recognized as strategically important energy consumers whose design choices can influence power system operation, sustainability targets, and long-term infrastructure planning.

In response to this increasing relevance, significant research efforts have focused on understanding data centers not only as IT facilities but also as energy-intensive systems that interact with electrical grids. Surveys and taxonomies emphasize the need for holistic approaches that jointly consider computing performance, energy efficiency, power quality, and reliability [2]. This system-level view has gradually shifted the perception of data centers from isolated facilities to active components of the broader energy ecosystem.

Figure 3 illustrates the evolution of green cloud computing, showing how research and design focus has progressively shifted from basic energy awareness towards more comprehensive energy-efficient techniques in cloud data centers. The figure highlights the transition from isolated hardware-level optimizations to integrated approaches that combine virtualization, resource management, and sustainability considerations, reflecting the growing importance of reducing energy consumption and environmental impact in large-scale cloud infrastructures [3].

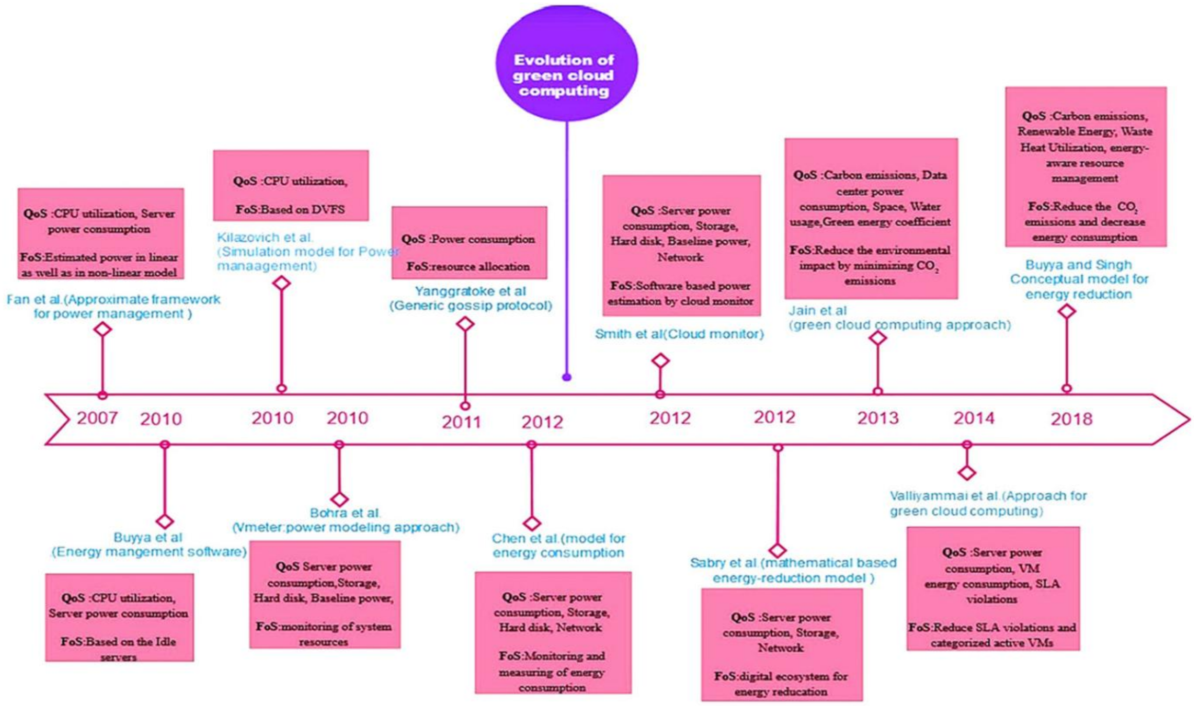

Figure 3. Evolution of green cloud computing

In summary, a data center is an integrated infrastructure that enables the delivery of digital services through the coordinated operation of IT equipment with supporting power and cooling systems. The importance originates from the leading role of data centers in modern society, its economic impact, and its growing influence on energy consumption and sustainability. These aspects provide the fundamental motivation for investigating data center architectures and for analyzing how power distribution choices affect efficiency, reliability, and future scalability.

2.2. Growth of Data Centers in Recent Years

The demand for data center services has increased significantly over the past decade, driven by the widespread use of cloud computing, digitalization of industrial and commercial processes, and the rapid growth of data intensive applications. Services such as online platforms, financial transactions, remote work infrastructures, and scientific computing increasingly rely on centralized and hyperscale data centers to ensure performance, scalability, and availability. As a result, both the number and the size of data centers have grown, leading to a substantial increase in installed IT capacity worldwide [7].

Recent studies show that the overall energy demand of data centers continues to rise drastically as shown in Figure 4. This trend is particularly evident with the expansion of artificial intelligence, machine learning, and high-performance computing workloads, which are characterized by high power densities and continuous operation [8]. These applications have shifted data center design priorities toward higher power availability per rack and more robust electrical and thermal infrastructures.

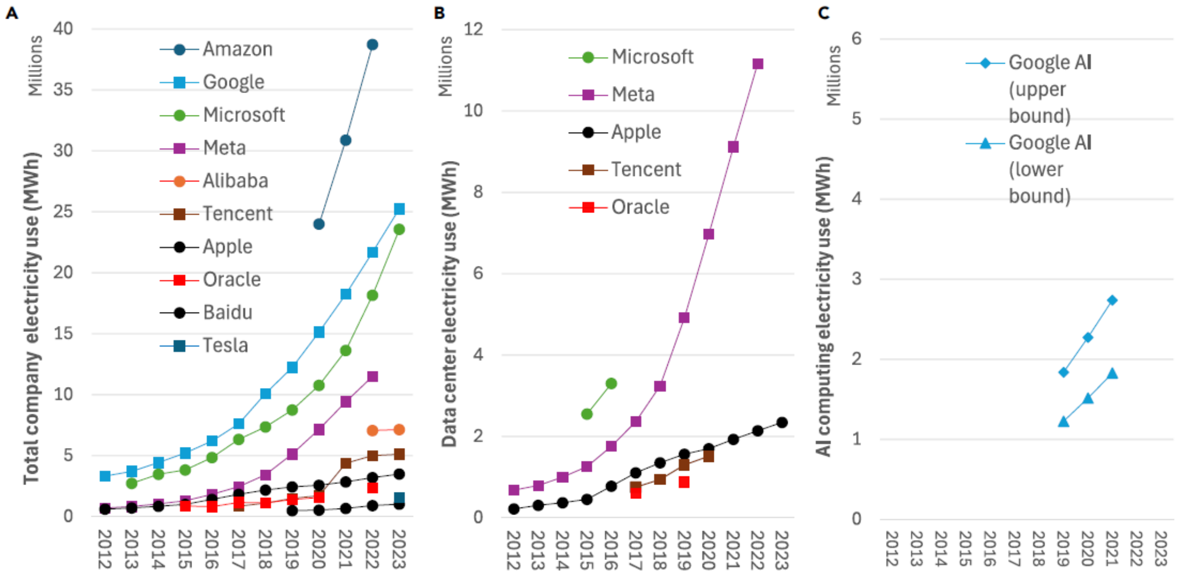

Figure 4. Electricity consumption of technology companies, data centers, and AI computing

At the same time, a significant uncertainty in estimating the actual energy consumption and growth rate of data centers is present. Differences in modeling assumptions, system boundaries, and data availability have led to a wide range of reported figures at national and global levels [6]. This uncertainty does not diminish the relevance of data centers as major electricity consumers; rather, it underlines the complexity of accurately quantifying their impact and forecasting future demand.

Comprehensive reviews of energy use models indicate that future growth in data center energy consumption will strongly depend on both technological progress and operational practices. While efficiency gains in IT equipment and infrastructure can partially offset demand growth, these improvements alone may not be sufficient to counterbalance the increasing scale and intensity of digital services [9]. Consequently, data centers are expected to remain a growing and structurally important load within electrical power systems.

2.3. New Improvements in Data Centers

The continuous growth in data center capacity and power density has driven significant research and development efforts aimed at improving both energy efficiency and environmental sustainability. Recent studies show that these improvements can be broadly classified into two main areas: advancements in thermal management and heat recovery, and innovations in energy systems including renewable integration and operational flexibility.

2.3.1. Cooling Technologies and Heat Reuse

Cooling systems represent a substantial portion of total data center energy consumption, particularly in facilities with high rack power densities. Traditional air-based cooling approaches face limitations as server power density increases, leading to reduced efficiency and higher operational costs. As a result, recent studies have increasingly focused on alternative cooling technologies that can better accommodate modern IT loads [10].

One of the most prominent developments is the adoption of direct liquid cooling solutions, where heat is removed directly at the server or component level. Liquid cooling offers significantly higher heat transfer capability compared to air cooling, enabling higher rack densities and more stable thermal conditions [11]. Survey based studies indicate that, while adoption is still limited to specific use cases such as high-performance computing and artificial intelligence workloads, interest in liquid cooling is rapidly increasing due to its potential efficiency benefits [12].

In parallel, there has been growing interest in the recovery and reuse of waste heat generated by data centers. Instead of dissipating heat to the ambient environment, several studies propose integrating data centers with district heating networks or local thermal loads, as shown in Figure 5, thereby improving overall energy utilization [13]. Such approaches are particularly attractive in urban environments, where recovered heat can contribute to space heating or industrial processes. A recent work discussed by Zhang *et al*. shows Waste Heat Recovery (WHR) pathways for data centers (Figure 6) and further highlights that WHR can play a key role in reducing the carbon footprint of data centers and supporting broader decarbonization strategies [14]. Beyond on-site utilization, data centers can support external thermal networks by regulating waste heat recovery through workload scheduling, while maintaining Quality of Service (QoS) requirements [15].

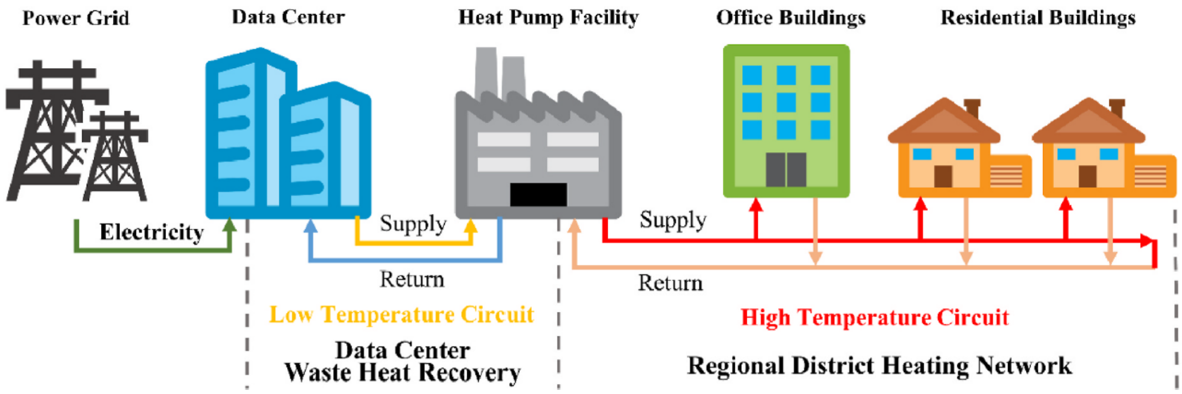

Figure 5. WHR in data centers

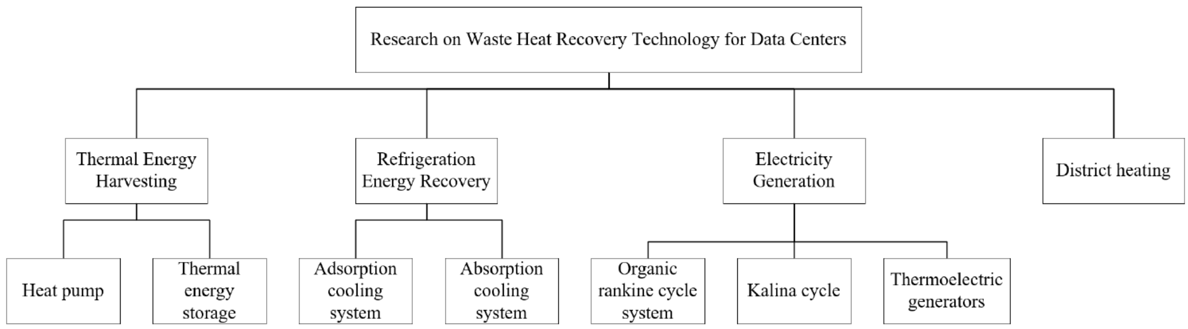

Figure 6. Conceptual framework of WHR pathways for data centers

2.3.2. Energy Systems, Renewables, and Operational Flexibility

Beyond thermal improvements, modern data center design increasingly considers the interaction between the facility and the electrical power system. Data centers are no longer solely passive loads, but they are active participants in integrated energy systems that include on-site generation, energy storage, and advanced control strategies [16].

The integration of renewable energy sources, such as photovoltaic systems, has been widely studied to reduce operational emissions [17]. However, the variability of renewable generation introduces challenges related to power balance and reliability. To address these issues, a recent literature explores data center microgrids that combine renewables, battery storage, and grid connection in an optimized manner [18]. These configurations allow data centers to improve energy resilience while reducing dependence on the external grid.

In addition to infrastructure level solutions, several studies emphasize the role of operational strategies in improving sustainability. Load shifting techniques, which relocate computation in time or space to periods or locations with lower carbon intensity, are effective tools for reducing emissions without major hardware changes [19]. Similarly, carbon aware scheduling and data transfer strategies aim to align computational demand with cleaner energy availability, further enhancing the environmental performance of data center operations [20].

Overall, the literature indicates that recent improvements in data center design extend well beyond incremental efficiency gains. Advances in cooling technologies, heat reuse, renewable integration, and operational control collectively reflect a shift toward viewing data centers as integrated components of the energy system. These developments also influence power distribution requirements and constraints, reinforcing the importance of evaluating alternative electrical architectures, such as DC-based systems, in the context of next-generation data centers.

2.4. Limitations of AC Systems Compared to DC

The choice of power distribution architecture is a fundamental design decision in data centers, as it directly affects energy efficiency, reliability, scalability, and compatibility with modern IT loads. Traditionally, data centers have relied on alternating current (AC) distribution, primarily due to historical grid standards and the widespread availability of AC equipment. However, the increasing power density of IT loads and the growing emphasis on energy efficiency have motivated a critical reassessment of this conventional approach. As a result, comparing AC and DC power distribution architectures has become a relevant and active area of research [21].

One of the main motivations for analyzing AC versus DC distribution lies in the structure of the power conversion chain. In typical AC-based data centers, electrical power undergoes multiple conversion stages, including rectification, inversion, and voltage transformation before reaching the IT equipment. Each conversion stage introduces losses, increases system complexity, and may reduce overall reliability [22]. Studies have shown that these cumulative losses can represent a significant fraction of total infrastructure energy consumption, particularly in large-scale facilities [23], [24].

In addition to conversion losses, AC-based data centers are affected by several power quality issues that arise from the nonlinear nature of IT loads. Modern servers and power supplies draw non sinusoidal currents, which generate harmonic distortion in the electrical network. These harmonics can lead to increased losses in conductors and transformers, excessive neutral currents in three-phase systems particularly due to harmonic components [25], and elevated thermal stress on electrical components [26]. Such effects complicate system design and often require oversizing of equipment or the use of additional mitigation measures [27].

The presence of harmonics and unbalanced currents in AC systems has also been shown to negatively impact transformer performance. Under non-sinusoidal voltage and current conditions, transformer losses and heating can increase beyond nominal values, potentially reducing equipment lifetime and operational efficiency [28], [29]. These phenomena are particularly relevant in data centers, where high load factors and continuous operation exacerbate thermal and aging effects.

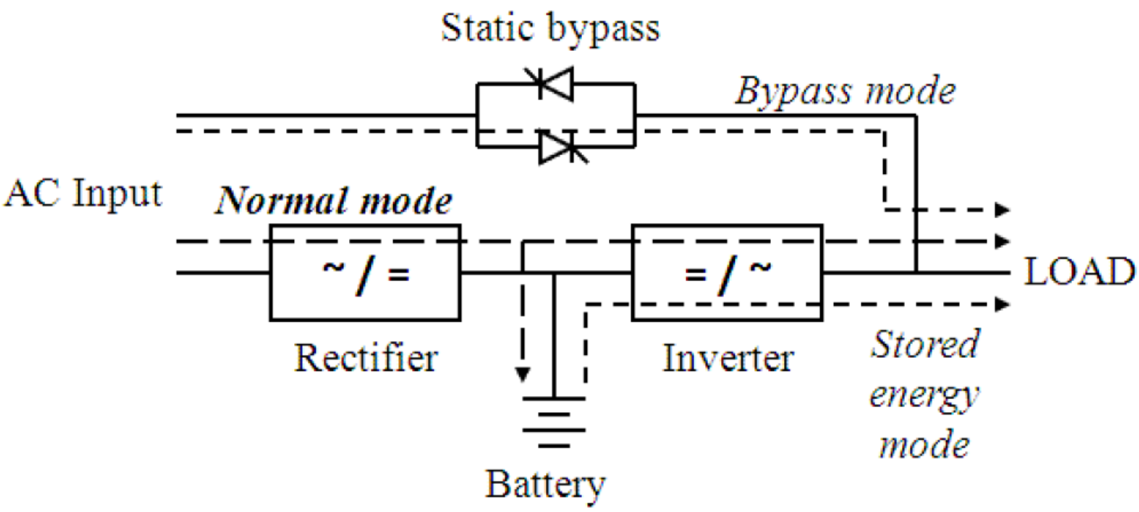

Figure 7. Block diagram for a double conversion UPS

Another limitation of AC-based architecture is related to Uninterruptible Power Supply (UPS) systems, which are essential for ensuring high availability. Double-conversion UPS systems, commonly used in data centers to provide high power quality, introduce additional conversion losses, and contribute to overall system inefficiency. A Block diagram for a double conversion UPS is shown in Figure 7 [30]. While high-efficiency operating modes exist, they often involve trade-offs between efficiency and power quality, further highlighting the inherent complexity of AC-based solutions [31].

These limitations of conventional AC distribution have motivated the investigation of alternative power-distribution architectures for data centers, particularly DC solutions, which aim to reduce conversion stages, distribution losses, and conductor requirements while maintaining high reliability.

Against this background, DC power distribution is an alternative architecture that may compensate for several of these limitations. By reducing the number of power conversion stages and supplying power in a form that is inherently compatible with electronic loads, green energy, and energy storage systems DC distribution has the potential to improve efficiency and simplify system design. A numerical efficiency analysis is done by Klemola for both AC and DC rack feeders, focusing on harmonic elimination and reduction in conversion stages, the result is shown in Figure 8 [32]. This figure shows a 6% to 13% improvement from AC to DC which directly translates into lower electrical losses, reduced cooling demand, and improved energy utilization at the data center.

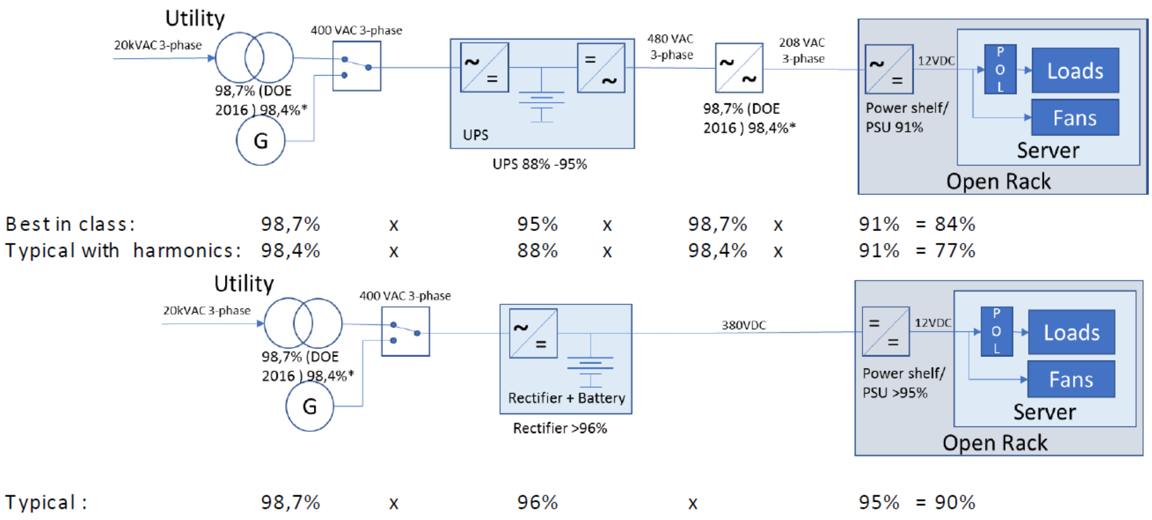

Figure 8. AC vs. DC efficiency comparison

These characteristics make DC architecture particularly attractive in data centers with high penetration of renewable energy sources and battery storage, where power is generated and stored in DC form.

In summary, the comparison between AC and DC power distribution in data centers is motivated by both efficiency considerations and the operational challenges associated with conventional AC systems. Power quality issues, conversion losses, and infrastructure complexity in AC-based architecture provide a strong technical rationale for investigating DC alternatives. This literature-based motivation forms the foundation for the quantitative analyses and comparative evaluations presented in the subsequent chapters of this thesis.

2.5. DC Distribution: Advantages, Architectures, and Standards

DC power distribution has emerged as a promising alternative to conventional AC-based architectures in data centers, particularly in the context of increasing power density, efficiency requirements, and integration of renewable energy sources. One of the primary advantages of DC distribution is the reduction in the number of power conversion stages between the utility grid and the IT loads. In DC systems, power can be distributed after a single rectification stage, thereby avoiding multiple AC–DC and DC–AC conversions that are typical of traditional architectures [33]. This reduction in conversion stages directly translates into lower electrical losses and potentially higher overall system efficiency.

Another important advantage of DC distribution lies in its inherent compatibility with modern data center loads and energy storage systems. Servers, network equipment, batteries, and photovoltaic systems all operate internally on DC. Supplying power in DC form reduces the need for internal rectifiers within IT equipment and simplifies the integration of battery energy storage systems at various levels of the power distribution chain [32]. As a result, DC architecture can offer a more direct and efficient power path from the source to the load.

From a reliability perspective, several studies indicate that DC distribution can simplify system topology and reduce the number of active components, which may lead to improved availability. Reliability analyses comparing AC and DC architectures show that eliminating inverters and reducing conversion equipment can decrease the number of potential failure points, particularly in UPS paths [33]. Shrestha et al. compares the conventional 480V AC power distribution and 380V DC power distribution architectures that is demonstrated in Figure 9 and Figure 10, respectively, resulting in around 5% efficiency improvement and 40% lower failure rate (for 2N redundancy) from AC to DC. This aspect is especially relevant for large scale data centers, where system complexity and redundancy levels have a significant impact on both reliability and Cap-Ex.

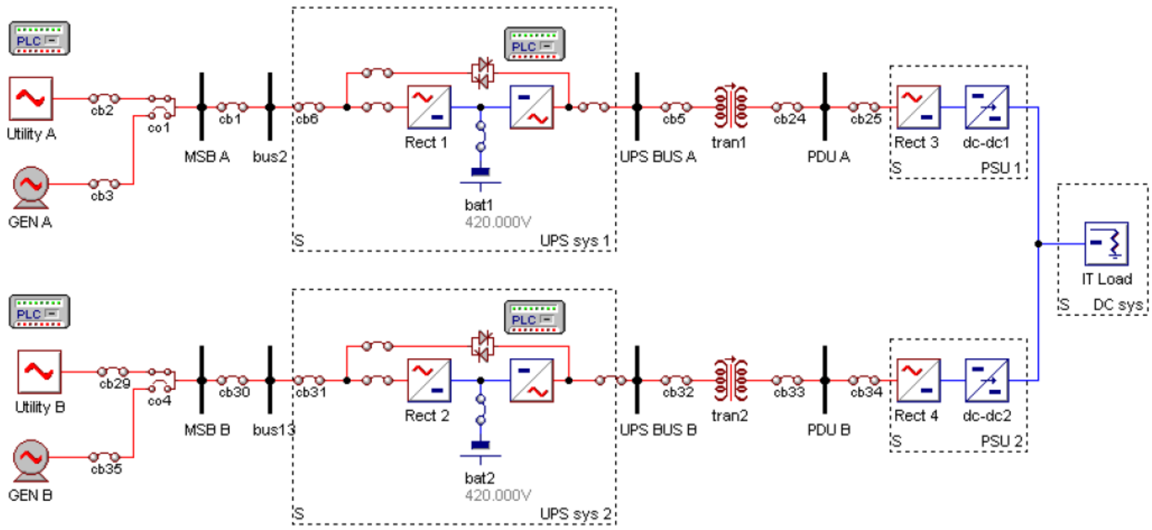

Figure 9. Simulation model of 480 V AC (2N topology)

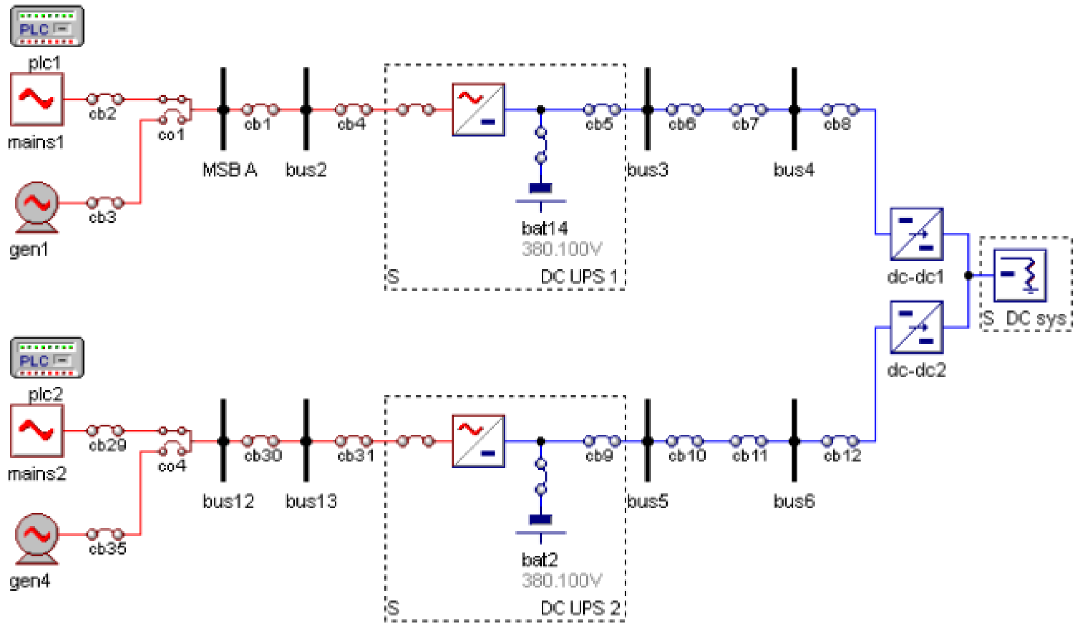

Figure 10. Simulation model of 380 V DC (2N topology)

In addition to conversion chain simplification, DC distribution can be implemented through different bus structures, commonly classified as radial, ring, ladder, and meshed configurations shown in Figure 11. These structures represent a direct trade-off between implementation cost/component count and supply continuity: radial structures are simplest but least tolerant to bus faults, while ladder and meshed structures improve fault isolation and continuity at the expense of higher complexity and cost. For critical loads, ladder or meshed structures are often considered attractive options when higher distribution level resilience is required [34].

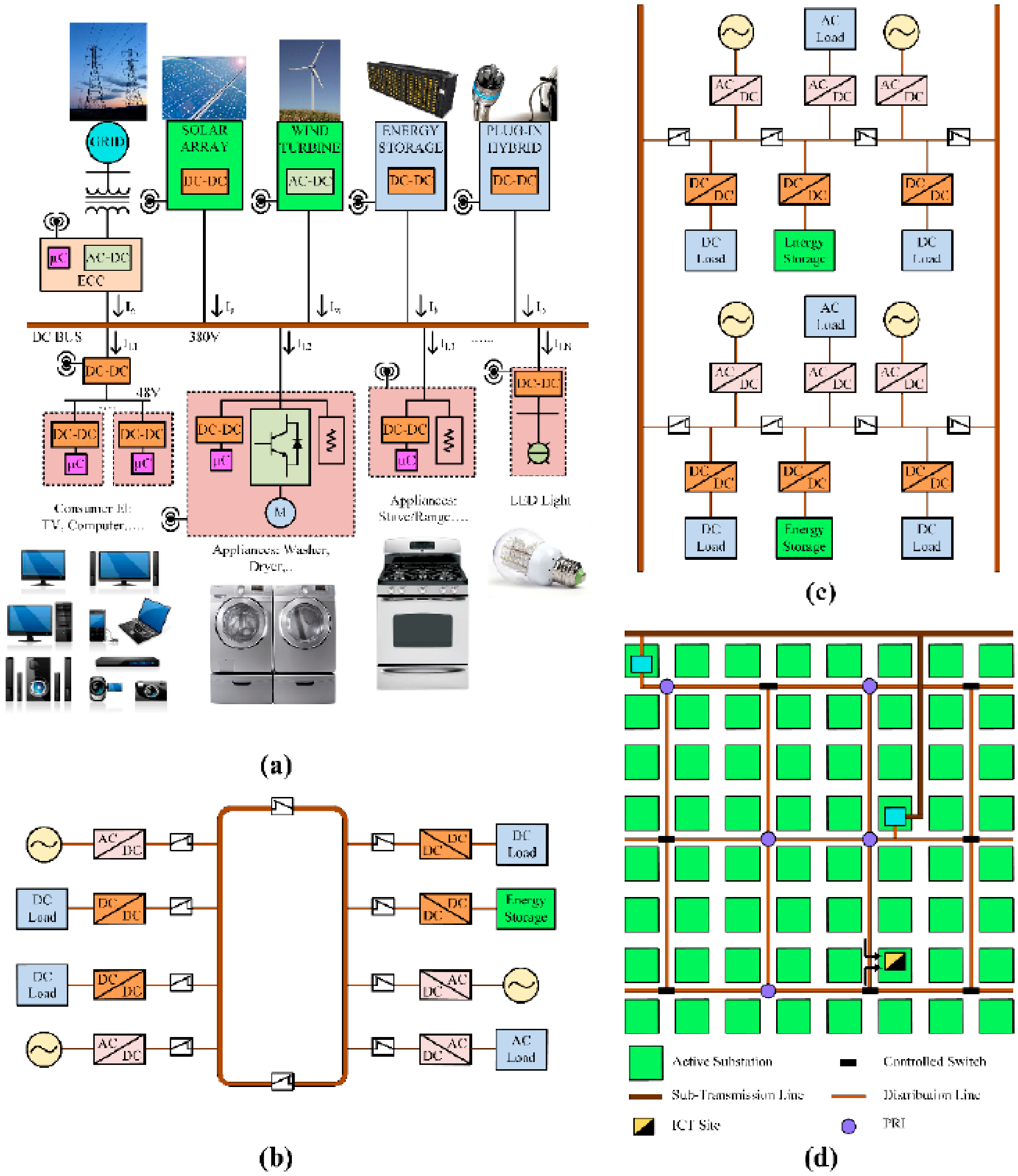

Figure 11. DC bus structures: (a) radial; (b) ring; (c) ladder; (d) meshed.

The most widely discussed implementation of DC distribution in data centers is based on medium voltage DC levels, typically around 380 - 400 V DC. Comprehensive architectural studies describe several possible configurations for 380 V DC data centers, differing mainly in the placement of rectifiers, battery systems, and point-of-load converters [35]. These architectures allow flexibility in system design while maintaining the benefits of DC distribution.

Standardization plays a crucial role in enabling the practical deployment of DC data center architecture. Technical specifications and interface standards define voltage ranges, grounding concepts, protection requirements, and interoperability between equipment from different manufacturers. Experimental and pilot installations further demonstrate that DC systems can be safely and reliably operated in commercial and industrial settings [36].

Several documents provide guidance on DC power interfaces and distribution concepts for data centers and telecom environments, supporting the feasibility of large-scale DC adoption [37], [38]. In the literature [37], Darla and Chitra provide a clear breakdown of how a data center's electrical input is allocated between the IT load and supporting overheads. Their data center power consumption breakdown figures (Figure 12. a, b) highlight that with DC, it is estimated that the power loss is reduced by about 14%. These two figures are useful in this thesis to motivate why distribution architecture (and especially reduced conversion) matters when evaluating AC versus bipolar DC solutions in large scale facilities.

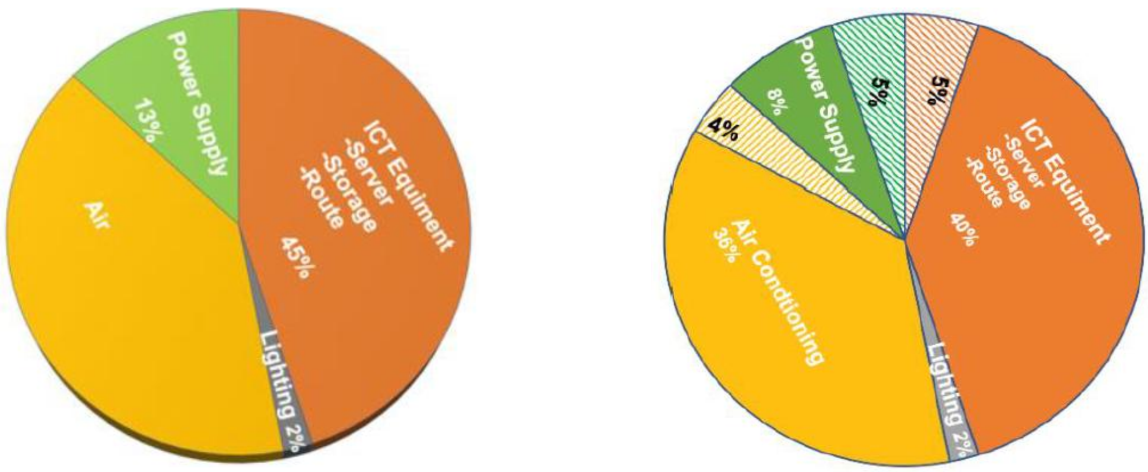

a) Conventional AC architecture

b) DC architecture

Figure 12. Data center power consumption breakdown

In addition, research on LVDC systems contributes to the understanding of protection, control, and modeling challenges associated with DC distribution. Modeling studies highlight the differences between AC and DC fault behavior and emphasize the need for dedicated protection strategies tailored to DC systems [39]. These findings are essential for ensuring safe operation and regulatory compliance as DC architecture evolves.

Experimental and field-oriented studies on ±380 V DC distribution report significantly lower cable losses compared to equivalent 400 V AC systems, under comparable loading assumptions [40]. In addition to the commonly discussed 380 - 400 V DC architectures, higher voltage DC distribution levels, such as 800 V DC, have recently attracted increasing attention for large scale data centers with high power demand. By increasing the distribution voltage, the current required for a given power level is reduced, leading to lower conduction losses, smaller conductor cross sections, and improved power density in distribution components. These advantages are particularly relevant in data centers characterized by long cable runs and high rack level power requirements, where resistive losses and copper usage represent key design constraints [35].

In this context, a bipolar 800 V DC configuration, typically implemented as ±400 V with respect to a neutral conductor, provides additional technical benefits compared to unipolar DC systems. Such architectures allow flexible load connection, reduced neutral currents under balanced operation, and improved fault tolerance, as partial operation can be maintained in the event of a single pole failure [41]. Owing to these characteristics, bipolar high voltage DC distribution represents a natural extension of existing DC architecture.

For these reasons, a bipolar 800 V DC power distribution approach is adopted and analyzed in this study. Figure 13 illustrates a representative implementation of a bipolar ±400 V (800 V DC) distribution for data centers, where an upstream conversion stage feeds a DC bus facility and power is then distributed to rack level PDUs and server power supplies through DC/DC conversion [17]. The figure also highlights how energy storage systems and on-site generation can be coupled directly to the same DC bus, which is consistent with the motivation of this thesis: reducing conversion stages and enabling a simpler power path for IT loads when adopting bipolar 800 V DC distribution. This choice enables a consistent evaluation of efficiency, conductor sizing, and reliability under conditions representative of next-generation data centers with increasing power density and stringent performance requirements.

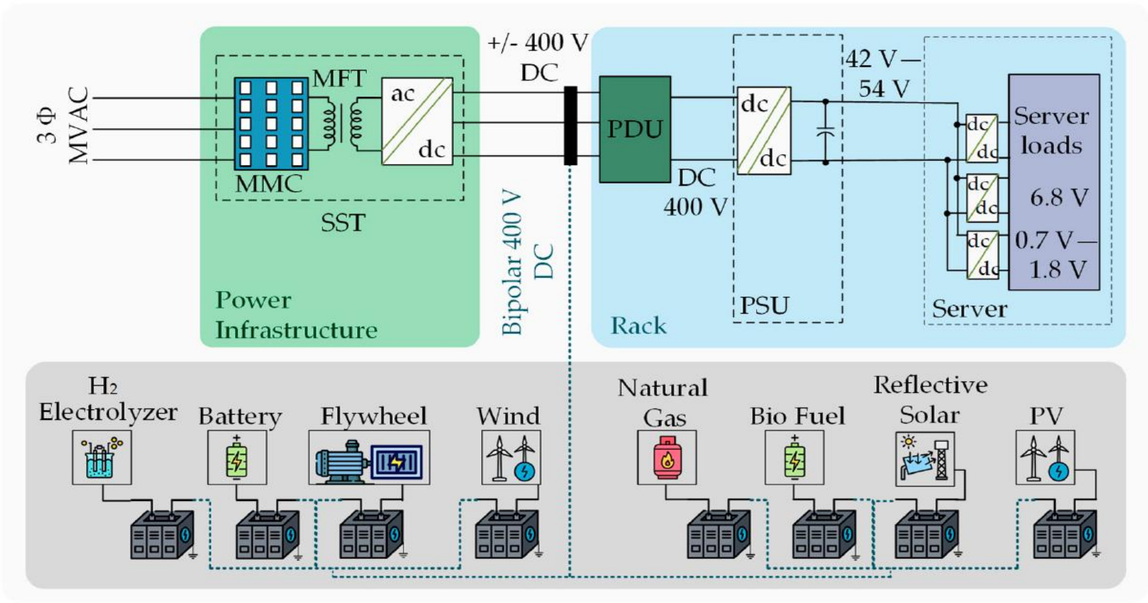

Figure 13. Data center facility with a bipolar ± 400 V DC distribution

In summary, DC power distribution offers multiple potential advantages over traditional AC systems in data centers, including improved efficiency, simplified power paths, enhanced compatibility with modern loads, and opportunities for improved reliability. Supported by emerging standards and validated through architectural studies and pilot deployments, DC-based solutions represent a technically viable option for next generation data centers. Figure 14, derived from [38], presents a weighted comparison of the main motivations for considering DC as opposed to AC architecture. This literature foundation supports the detailed comparative analysis between AC and DC power distribution architectures developed in the following chapters of this thesis.

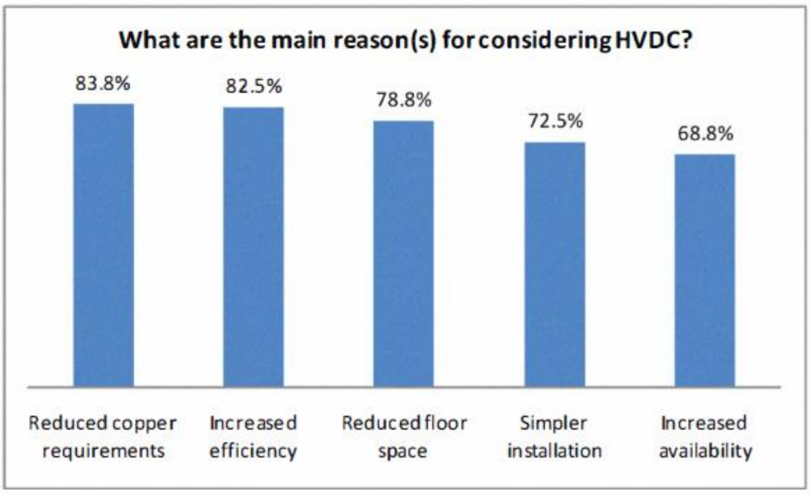

Figure 14. Main reasons for considering DC.

It should be noted that the terminology used in Figure 14 follows the convention adopted in the referenced telecommunication literature, where 800 V DC systems are categorized under the term HVDC. In the context of classical power system engineering, however, HVDC typically refers to high-voltage transmission systems operating at voltage levels in the order of hundreds of kilovolts. In this thesis, the 800 V DC architecture investigated is considered a low-voltage DC (LVDC) distribution system, consistent with electrical power engineering standards. The use of the term HVDC in the referenced figure therefore reflects sector-specific nomenclature rather than transmission-level voltage classification.

3 Copper Usage, DC sizing & Pricing

3.1. Scope & Inputs

This section defines the sizing methodology and cost estimation approach adopted for the existing AC and the proposed DC distribution models. The analysis starts with the MV/LV transformer, then proceeds through the UDP bus, UPS/ battery system, PDU bus, and RPP level, terminating at the DC load (rack level), with each bus indicating a distinct level of analysis.

Both models are evaluated under identical routing and load conditions to ensure a fair comparison in terms of conductor sizing, copper mass, and cable cost.

The analysis considers all low voltage distribution lines supplying the IT loads, including the lines feeding the Load Bank (LB), while feeders serving mechanical loads are excluded, as these lines must remain AC and will not contribute to the AC vs. DC comparison done in this study. For each relevant line, conductors belonging to all three phases, the neutral, and the Protective Earth (PE) are included.

Redundancy assumptions follow a 2N redundancy model for the IT load and a 3-to-make-2 redundancy scheme for all other system components. Sizing is performed under worst case operating conditions; meaning that the analysis assumes that if there is a fault or maintenance in a specific part of the system, the operating part of the distribution path must be capable of supplying the full load corresponding to the nominal capacity.

In the DC architecture, two conductor-sizing approaches are considered. The first approach selects the minimum possible cable cross-sectional area (CSA) that satisfies both ampacity and voltage-drop limits, and it represents the lowest-copper solution.

The second approach sizes DC conductors to maintain a current density comparable to the AC reference (constant *J*), providing a more conservative thermal margin.

The main design limits and assumptions adopted in this study are summarized as follows:

- The allowable steady state voltage drop is limited to 1.6% for each level.
- Conductor ampacity, resistance, and inductance are evaluated assuming single core cables. FG7M1 cables (0.6/1 kV AC) are used for the AC configuration, while FG16R16 cables (1.5 kV DC) are adopted for the DC configuration.
- Ampacity tables for AC and DC cables are reported in Table 1 and Table 2, respectively.
- Cable pricing is derived from the ComCavi shop, based on October 2025, and expressed in €/m as a function of conductor Cross Sectional Area (CSA).
- System configurations and cable routings are extracted from design drawings and Single Line Diagrams (SLDs). The load distribution is assumed to be homogeneous, with each endpoint assigned the same power demand.
- For both the AC and DC configurations, Neutral (N) and PE conductors are included in the calculations. In this case, the neutral conductor is present only at the RPP level, while the PE conductor is considered at all distribution levels.

Table 1. Ampacity table for AC cables

Size [number × mm2]	cable weight [kg/km]	Max. electrical resistance at 20°C [Ω/km]	Current rating in pipe in air at 30°C [A]
1 x 10	150	1.91	66.0
1 x 16	205	1.21	88.0
1 x 25	295	0.798	117.0
1 x 35	390	0.554	144.0
1 x 50	550	0.386	175.0
1 x 70	740	0.272	222.0
1 x 95	940	0.206	269.0
1 x 120	1210	0.161	312.0
1 x 150	1490	0.129	355.0
1 x 185	1850	0.106	417.0
1 x 240	2350	0.0801	490.0
1 x 300	2950	0.0641	-

Table 2. Ampacity table for DC cables

Size [number × mm2]	Cable weight [kg/km]	Max. electrical resistance at 20°C [Ω/km]	Current rating in pipe in air at 30°C [A]
1 x 1.5	55	13.3	20.0
1 x 2.5	66	7.98	28.0
1 x 4	84	4.95	37.0
1 x 6	110	3.30	48.0
1 x 10	150	1.91	66.0
1 x 16	220	1.21	88.0
1 x 25	310	0.798	117.0
1 x 35	410	0.554	144.0
1 x 50	560	0.386	175.0
1 x 70	760	0.272	222.0
1 x 95	960	0.206	269.0
1 x 120	1210	0.161	312.0
1 x 150	1480	0.129	355.0
1 x 185	1790	0.106	417.0
1 x 240	2320	0.0801	490.0
1 x 300	2840	0.0641	-
1 x 400	3735	0.0486	-

The AC and DC cable data reported in Table 1 and Table 2 show that, for the same conductor cross-section, the electrical resistance at 20 °C and the current carrying capacity under identical installation conditions are identical. This confirms that the thermal and resistive behavior of the cables is determined by conductor size and material, rather than by the nature of the current. The main difference lies in the available size range, as DC cable catalogs typically offer both smaller and larger cross-sections, providing greater flexibility for optimized conductor selection in DC power distribution systems.

3.2. AC Configuration

In this section, the voltage drop for the existing AC distribution configuration is described.

Line data are extracted from the available SLDs and design tables. For each line, the following parameters are collected: line identifier, CSA [mm^2], length [m], number of parallel lines, resistance per unit length [$\frac{\Omega}{km}$], and reactance per unit length [$\frac{\Omega}{km}$].

3.2.1. Voltage Drop Calculations

In this section, the line-to-line voltage drop is evaluated for the AC distribution configuration and later compared with the DC alternative. For three-phase AC feeders, the steady state line-to-line voltage drop depends on the conductor's resistance (R) and reactance (X), the operating current (I), and the cable length (L). The following expressions are adopted to evaluate the worst-case voltage drop under rated load conditions.

The current calculation is performed under worst-case operating conditions feeding the design load. The system is modeled as a hierarchical structure composed of multiple distribution levels (e.g., UDP → UPS → PDU → RPP), as shown in Figure 2. At each level ℓ, the design load is obtained by uniformly distributing the total IT power among the identical devices operating at that level.

Let P_{IT} be the total IT power demand and N_ℓ the number of parallel loads at level ℓ. The assigned power and nominal current for each unit are given by:

$$P_\ell = \frac{P_{IT}}{N_\ell}$$

$$I_{\ell,nom,AC} = \frac{P_\ell}{\sqrt{3} \times V_{AC} \times \cos(\varphi)} = \frac{P_{IT}}{N_\ell \times \sqrt{3} \times V_{AC} \times \cos(\varphi)}$$

At levels where multiple identical three phase cable sets are used in parallel, the current carried by each set is obtained as:

$$I_{\ell,set,AC} = \frac{I_{\ell,nom,AC}}{N_{sets}}$$

Where N_{sets} is the number of parallel three phase cable sets.

In this analysis, the line-to-line AC voltage is assumed equal to $V_{AC} = 400\,V$, and the load power factor is $\cos(\varphi) = 0.95$.

The above formulation applies to all distribution levels except for feeders supplying the UPS units, which require additional considerations. To compute the maximum upstream current of the UPS, the following worst-case assumptions are adopted:

- UPS efficiency: $\eta = 0.96$,
- Battery recharge rate: $r = 20\%$,
- Load power factor: $\mathrm{pf_{load}} = 0.95$,
- UPS input power factor: $\mathrm{pf_{in}} = 0.96$.

The battery recharge rate is assumed to be 20% to represent a worst-case condition, such as immediately following a supply interruption or fault. Under normal operating conditions, the recharge rate is typically lower and commonly ranges between 5% and 10%.

The relationship between UPS output and input currents is expressed as:

$$I_{\mathrm{in,\ UPS}} = I_{\mathrm{out,UPS}} \times \frac{\mathrm{pf_{load}}}{\eta\ \mathrm{pf_{in}}}\ (1 + r)$$

With the adopted parameters, the resulting input current is:

$$I_{\mathrm{in,\ UPS}} = I_{\mathrm{out,\ UPS}} \times 1.237$$

Indicating that, under worst-case condition, the UPS input current is approximately 24% higher than the output current.

To account for redundancy, a level dependent multiplier $k_{\ell,red}$ is applied, assuming the surviving path must carry the full load under fault or maintenance conditions. The resulting worst-case design current is therefore:

$$I_{\ell,worst,AC} = k_{\ell,red} \times I_{\ell,set,AC}$$

Where $k_{\ell,red}$ is 1.5 in case of 3 to make 2 redundancies, and 2 in case of 2N redundancy.

The line-to-line voltage drop is then calculated using the following expression:

$$\Delta V_{LL,\ell,AC} = \sqrt{3} \times I_{\ell,worst,AC} \times (R_{\ell,\theta,AC} cos(\varphi) + X_\ell sin(\varphi)) \times L_\ell \times 0.001$$

where:

- L is the cable length [m].
- X is the positive sequence inductive reactance per kilometer, assumed temperature independent and taken from manufacturer data [Ω/km].
- R_θ is the conductor resistance per kilometer at operating temperature θ [Ω/km].
- $\cos(\varphi) = 0.95$, yielding $\sin(\varphi) = \sqrt{1 - 0.95^2} = 0.312$.

The conductor resistance at temperature θ is derived from the reference value at 20°C (R_{20}) as:

$$R_\theta = R_{20}\big(1 + \alpha(\theta - 20)\big)$$

With a temperature coefficient $\alpha = 0.00404\ °C^{-1}$. A conductor temperature of 75 °C is assumed for cables supplying the RPPs, while 70 °C is assumed for cables at the PDU and UDP levels.

The voltage drop percentage is finally obtained as:

$$VD_{\ell,AC}\% = \frac{\Delta V_{LL,\ell,AC}}{400} \times 100$$

3.3. DC Sizing Methodology for minimum CSA

This section describes the methodology adopted for sizing the DC distribution conductors considered in this study. The procedure follows an iterative approach based on two design constraints: conductor ampacity and voltage drop compliance.

First, the worst-case DC current $I_{\mathrm{dc,worst}}$ is compared against the allowable current I_b of a candidate cable as specified in the ampacity table for DC rated conductors (Table 2). A cable CSA is considered acceptable if the following conditions are satisfied:

$$I_{\mathrm{dc,worst}} \leq I_b$$

Once the ampacity criterion is fulfilled, the corresponding voltage drop is evaluated and verified with the design limits defined in Section 3.1. If the voltage drop requirement is not satisfied, a cable with a larger CSA is selected and the verification procedure is repeated. This iterative process continues until both criteria are simultaneously met.

3.3.1. Worst-Case Current Calculation

The calculation of DC currents follows the same approach adopted for the AC configuration. The distribution system is modeled as a hierarchical structure composed of multiple levels (e.g., UDP → PDU → RPP), as shown in Figure 1 b. At each level ℓ, the total IT power is uniformly distributed among the loads operating at that level.

Let P_{IT} be the total IT demand and N_ℓ the number of parallel loads at level ℓ and $V_{\mathrm{DC}} = 800$ V is the nominal distribution DC voltage. The assigned power and nominal current for each unit are given by:

$$P_\ell = \frac{P_{\mathrm{IT}}}{N_\ell}$$

$$I_{\ell,\mathrm{nom,DC}} = \frac{P_\ell}{V_{\mathrm{DC}}} = \frac{P_{\mathrm{IT}}}{N_\ell\, V_{\mathrm{DC}}}$$

At levels where multiple parallel DC circuits are installed, the current carried by each circuit is obtained as:

$$I_{\ell,\mathrm{set,DC}} = \frac{I_{\ell,\mathrm{nom,DC}}}{N_{\mathrm{sets}}}$$

where N_{sets} is the number of parallel DC cable sets. Since DC architecture is considered consistent with the AC configuration, some variables have the same value in both AC and DC calculations (P_{IT}, N_{ℓ}, P_{ℓ}, N_{sets}).

For the battery interface, the relationship between battery output and input currents is expressed as:

$$I_{\mathrm{in,batt}} = \frac{I_{\mathrm{out,batt}}}{\eta_{\mathrm{batt}}} \times (1 + r)$$

where η_{batt} is the battery efficiency and r is the charging factor. Assuming a charging factor of $r = 20\%$ and a battery efficiency of $\eta_{\mathrm{batt}} = 97\%$, the resulting input current is:

$$I_{\mathrm{in}} = 1.237 \times I_{\mathrm{out}}$$

This indicates that, under worst-case conditions, the battery input current is approximately 24% higher than the output current, like AC configuration.

Redundancy is accounted for by applying the same contingency multipliers as the AC configuration:

$$I_{\ell,worst,DC} = k_{\ell,red} \times I_{\ell,set,DC}$$

3.3.2. Voltage Drop Criterion

Once the cable CSA satisfies the ampacity requirement, the voltage drop is evaluated to verify compliance with the design limits.

In bipolar DC distribution systems, voltage drop is evaluated along the complete go-and-return current path, as both conductors contribute to the total resistive drop. Unlike AC systems, reactive components are absent at steady state, and the voltage drop depends solely on the conductor's resistance, current, and route length.

For a two wire DC circuit, the steady-state voltage drop is calculated along the go-and-return path as:

$$\Delta V_{\ell,DC} = 2 \times I_{\ell,worst,DC} \times R_{l,\theta} \times L_{\ell} \times 0.001$$

where:

- $I_{\ell,\mathrm{worst}}$ is the worst-case current at level ℓ,

- $R_{\ell,\theta}$ is the conductor resistance per unit length at operating temperature θ
- L_ℓ is the one-way route length for level ℓ, expressed in meters.

This expression is particularly suitable for bipolar DC architectures, where current flows simultaneously in the positive and negative conductors.

The conductor resistance is evaluated at an operating temperature of 70 °C for cables at the UDP and PDU levels, and 75 °C for cables supplying the RPPs. Resistance values are derived from manufacturer data and corrected for temperature using the same approach adopted for the AC configuration.

The corresponding voltage drop percentage is calculated as:

$$\%\Delta V_{\ell,DC} = \frac{\Delta V_{\ell,DC}}{V_{DC}} \times 100$$

This percentage must not exceed the segment-specific voltage drop limits defined in Section 3.1.

3.4. DC Sizing Methodology for Constant J

In addition to the minimum CSA iterative procedure, a constant current density criterion is also evaluated for the DC architecture. For each distribution level ℓ, a reference AC current density is defined as:

$$J_{\ell,\mathrm{AC}} = \frac{I_{\ell,\mathrm{worst,AC}}}{CSA_{\ell,\mathrm{AC}}}$$

The corresponding DC conductor CSA for the constant-J case is then selected as the smallest standardized CSA that satisfies:

$$CSA_{\ell,\mathrm{DC},J} \geq \frac{I_{\ell,\mathrm{worst,DC}}}{J_{\ell,\mathrm{AC}}}$$

Since the CSA obtained from the constant current density criterion is, by definition, equal to or greater than the minimum CSA previously selected to satisfy ampacity and voltage-drop limits, the resulting voltage drop in the constant-J case is equal to or lower than that of the minimum-CSA design. Therefore, an additional voltage-drop verification is not required for this case. The constant-J configuration thus represents a thermally conservative DC design, whereas the minimum-CSA configuration corresponds to the lowest-copper solution.

3.5. Numerical Results

This section compares the AC and DC distribution architectures in terms of design current, CSA, and voltage drop performance. First, representative lines at each distribution level are analyzed as examples. Subsequently, the voltage drop results for all system lines are summarized, and the implications for copper usage and cable cost are discussed.

3.5.1. Design current, CSA, and Voltage Drop comparison

The total installed IT capacity of the site is assumed equal to $P_{IT} = 9.6$ MW. In the existing AC configuration, feeder segments are implemented using 240 mm² cables, while branches supplying the RPPs use 70 mm² conductors.

UDP Level

At the UDP level, AC feeders employ 240 mm² cables with lengths of 10 m and 15 m. A total of 12 UDPs are considered. The nominal currents are calculated as:

$$I_{1,\text{nom,AC}} = \frac{9.6 \times 10^6}{12 \cdot \sqrt{3} \cdot 400 \cdot 0.95} = 1215\text{ A}$$
$$I_{1,\text{nom,DC}} = \frac{9.6 \times 10^6}{12 \cdot 800} = 1000\text{ A}$$

Each distribution path consists of five parallel cable sets. Accounting for redundancy (3-to-make-2), the worst-case line currents are:

$$I_{1,\text{worst,AC}} = \frac{1215}{5} \cdot \frac{3}{2} = 364.5\text{ A}$$
$$I_{1,\text{worst,DC}} = \frac{1000}{5} \cdot \frac{3}{2} = 300\text{ A}$$

The DC current is approximately 18% lower than the AC value. Based on the FG16R16 ampacity data, the minimum acceptable DC cable size is 120 mm², corresponding to an ampacity of 312 A.

Considering the longest route (15 m), the resulting voltage drops are:

- AC: $\Delta V = 1.10$ V→ VD% $= 0.27\%$
- DC: $\Delta V = 1.74$ V→ VD% $= 0.22\%$

Despite the halved CSA, the DC configuration exhibits a lower voltage drop percentage.

For the constant current density criterion, the AC feeder is first used to determine the reference current density at this distribution level:

$$J_{\ell,AC} = \frac{I_{\ell,AC}}{CSA_{\ell,AC}} = \frac{364.5}{240} = 1.52\text{ A/mm}^2$$

The DC conductor cross-section required to preserve the same current density is then obtained from:

$$CSA_{\ell,DC,J} \geq \frac{I_{\ell,DC}}{J_{\ell,AC}} = \frac{300}{1.52} = 197 \text{ mm}^2$$

Based on the available standardized cable sizes in the ampacity table, the next admissible cross-section is 240 mm². This value coincides with the CSA used in the AC feeder at the same level.

Because the constant-J selection results in a cross-section greater than the minimum-CSA DC design (120 mm²), the associated voltage drop is inherently equal to or lower than that of the minimum-CSA case. Consequently, a separate voltage-drop recalculation is not necessary for this configuration.

UPS / Battery Feeders

At the same level, feeders supplying the UPSs (AC) and batteries (DC) are also evaluated. Worst-case currents, accounting for efficiency and charging assumptions, are:

$$I_{\text{UPS,nom}} = 1502 \text{ A}$$

$$I_{\text{batt,nom}} = 1237 \text{ A}$$

With six parallel cable sets and redundancy applied:

$$I_{\text{UPS,worst}} = 375.6 \text{ A}$$

$$I_{\text{batt,worst}} = 309.2 \text{ A}$$

The resulting voltage drops are 0.38% for AC and 0.30% for DC (with 120 mm^2 cables). Once again, the DC configuration achieves lower current and a lower voltage drop percentage with half the CSA.

For the constant current density approach, the reference AC current density at this level is calculated as:

$$J_{\ell,AC} = \frac{I_{\ell,AC}}{CSA_{\ell,AC}} = \frac{375.6}{240} = 1.56 \text{ A/mm}^2$$

The required DC conductor cross-section under the constant-J criterion is therefore:

$$CSA_{\ell,DC,J} \geq \frac{I_{\ell,DC}}{J_{\ell,AC}} = \frac{309.2}{1.56} = 198 \text{ mm}^2$$

Referring to the manufacturer ampacity table, the nearest standardized cross-section equal to or greater than this value is 240 mm².

PDU Level

At the PDU level, assuming 36 operational PDUs under worst-case condition and two parallel line sets per path, the currents are:

$$I_{2,\text{worst,AC}} = 304\ \text{A}$$

$$I_{2,\text{worst,DC}} = 250\ \text{A}$$

For DC, a 95 mm² cable satisfies the ampacity requirement but results in a voltage drop of 1.55% over a 100 m route. However, since the number is close to the allowable limit and the assumed cable length of 100 m is an approximation that may underestimate the actual routing distance, adopting a larger CSA of 120 mm² reduces the voltage drop to 1.21%, which is fully compliant with design criteria and is lower than the corresponding AC voltage drop percentage (1.53%). In addition, standardizing on a larger cross-section reduces the number of cable sizes required across the distribution network, which represents a significant advantage in terms of design simplicity and system standardization.

For completeness, the constant current density criterion is also applied at the PDU level. Using the AC feeder at this level as the reference, the current density is:

$$J_{2,AC} = \frac{304}{240} = 1.27\ \text{A/mm}^2$$

The corresponding DC cross-section required to preserve the same current density is:

$$CSA_{2,DC,J} \geq \frac{250}{1.27} = 197\ \text{mm}^2$$

According to the standardized cable sizes in the ampacity table, the next available value is 240 mm².

RPP Level

At the RPP level, AC branches use 70 mm² cables. Assuming 360 active RPPs for design purposes, the nominal currents are:

$$I_{3,\text{nom,AC}} = 40.54\ \text{A}$$

$$I_{3,\text{nom,DC}} = 33.33\ \text{A}$$

Applying 2N redundancy yields worst-case currents of 81 A (AC) and 66.7 A (DC). These currents and length of maximum 200 m led to a VD% of 2.4% for AC and 2.3% for DC with 35 mm^2 cables. In this case, while a 35 mm² DC cable satisfies the ampacity constraint, it leads to a voltage drop exceeding the design limit. Increasing the CSA to 50 mm² results in a compliant voltage drop of 1.57%.

It should be noted that the assumption of 360 simultaneously active RPPs, and the length of 200 m represent a design condition; in practical operation, these numbers are typically lower. Therefore, the worst case 1.57% voltage drop is acceptable, although it is close to the limit of 1.6%.

For the constant current density variant, the reference AC current density at the RPP level is:

$$J_{3,AC} = \frac{I_{3,worst,AC}}{CSA_{3,AC}} = \frac{81}{70} = 1.16 \text{ A/mm}^2$$

Accordingly, the required DC cross-section to maintain the same current density is:

$$CSA_{3,DC,J} \geq \frac{I_{3,worst,DC}}{J_{3,AC}} = \frac{66.7}{1.16} = 57.5 \text{ mm}^2$$

Based on the available standardized cable sizes, the nearest admissible CSA is 70 mm², same as the AC system.

The results show that, across all distribution levels, the DC configuration enables a consistent reduction in design current and voltage drop compared to the AC architecture.

- For minimum CSA approach, upstream feeder CSAs are reduced by 50%, while RPP branch CSAs are reduced by about 30%.
- For the constant J approach, the CSA is similar to the AC system, although considering that the DC architecture employs fewer conductors per circuit (two poles instead of three phases), also this approach leads to a reduction in overall copper usage and cable cost.

These findings provide the basis for the quantitative copper mass and cost comparison presented in the following subsections.

3.5.2. Voltage Drop Comparison

From the MV/LV transformer to the RPP level considered in this study, three possible electrical routes are seen from the rack point of view as shown in Figure 15, and described as:

- Route 1: MV/LV transformer → UPS bypass → UDP → PDU → RPP (four cable segments)
- Route 2: MV/LV transformer → UDP → PDU → RPP (three cable segments)
- Route 3: MV/LV transformer → UPS → UDP → PDU → RPP (four cable segments)

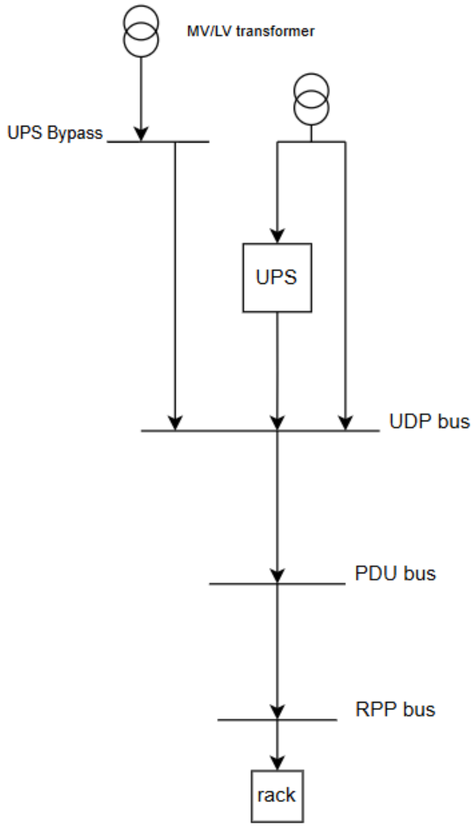

Figure 15. Electrical routes seen from the rack point of view

The calculated voltage drops for each cable segment at each level, and the corresponding values are reported in Table 3 for both AC and DC configurations in all the three possible routes.

From Table 3, Route 3 results in the highest voltage drop and therefore represents the worst-case condition for both architectures. In absolute terms, the DC configuration exhibits higher voltage drops expressed in volts. However, when normalized with respect to the system voltage, the resulting voltage drop percentage is consistently lower for DC architecture due to the doubled operating voltage level.

For all routes, the DC voltage drop percentage remains more than 1% lower than the AC configuration. This confirms that DC architecture provides improved voltage drop performance from a design perspective, having also smaller cables.

Table 3. Voltage-drop comparison

Routes	paths	AC		DC	
		ΔV [V]	VD%	ΔV [V]	VD%
Route 1	transformer --> UPS bypass	0.73	0.18%	0.966	0.12%
	UPS bypass --> UDP	0.73	0.18%	0.966	0.12%
	UDP --> PDU	6.1	1.53%	9.68	1.21%
	PDU --> RPP	9.69	2.42%	12.58	1.57%
	TOTAL	17.25	4.31%	23.45	2.93%
Route 2	transformer --> UDP	1.1	0.27%	1.74	0.22%
	UDP --> PDU	6.1	1.53%	9.68	1.21%
	PDU --> RPP	9.69	2.42%	12.58	1.57%
	TOTAL	16.89	4.22%	24	3%
Route 3	transformer --> UPS	1.5	0.38%	2.4	0.3%
	UPS --> UDP	0.73	0.18%	1.16	0.15%
	UDP --> PDU	6.1	1.53%	9.68	1.21%
	PDU --> RPP	9.69	2.42%	12.58	1.57%
	TOTAL	18.02	4.5%	25.82	3.22%

The voltage drop analysis confirms that the proposed DC architecture provides superior performance from the MV/LV transformer down to the RPP level. Although absolute voltage drops expressed in volts are higher for DC, the normalized voltage drop percentages are consistently lower than those of the AC system. This result is primarily driven by the higher voltage and reduced line currents of DC architecture. For all identified routes, the DC voltage drop margins remain within the adopted design limits while allowing smaller conductor cross sections. These findings demonstrate that DC distribution not only enables cable downsizing but also preserves robust voltage regulation across the entire distribution chain.

3.5.3. Copper Volume and Cable Mass Calculation

For a given cable route, the total number of conductors is defined as:

$$N_{\text{cond}} = n_{\text{par}} \times n_{\text{pole}}$$

where:

- n_{par} is the number of parallel cable sets,
- n_{pole} is the number of current carrying conductors per circuit (three phases for AC, two poles for DC).

The copper volume and copper mass associated with each line are calculated using the following expressions:

$$Vol_{cu,line} = \frac{CSA \times L \times N_{cond}}{10^6}$$

$$M_{\text{cu,line}} = L \times m \times N_{\text{cond}}$$

Where:

- CSA: Cross Section Area of the cable [mm^2]
- L: cable length [m]
- $Vol_{AC,line}$: copper volume of the line [m^3]
- m: manufacturer declared copper mass per meter for the selected CSA [kg/km].
- $M_{\text{cu,line}}$: cable mass of the line [kg]

The total copper volume and mass are therefore calculated as:

$$Vol_{total} = \sum_{lines} Vol_{cu,line}$$

$$M_{\text{Cu,tot}} = \sum_{lines} M_{Cu,line}$$

This formulation allows a direct comparison of total copper usage between the AC and DC distribution architectures.

3.5.4. Cable Cost Model

For the next step, cable pricing is obtained from “ComCavi” in October 2025. The analyzed system employs only single core cables with CSA of 240 mm² and 70 mm². At the time of the analysis, the corresponding unit prices for AC were 32.8 €/m for 240 mm² cables and 9.94 €/m for 70 mm² cables; and for DC cables the prices were 24.75 €/m for 240 mm² , 16.55 €/m for 120 mm², 9.93 €/m for 70 mm² , and 7 €/m for 50 mm² cables.

The total cable cost for one section is calculated as:

$$C_{AC} = \sum_{240mm2\ lines} 32.8 \times N_{cond} \times L + \sum_{70mm2\ lines} 9.94 \times N_{cond} \times L$$

$$C_{DC\_\text{min.CSA}} = \sum_{120mm2\ lines} 16.55 \times N_{cond} \times L + \sum_{50mm2\ lines} 7 \times N_{cond} \times L$$

$$C_{DC_{const\cdot J}} = \sum_{240mm2\ lines} 24.75 \times N_{cond} \times L \ + \sum_{70mm2\ lines} 9.93 \times N_{cond} \times L$$

The overall copper volume, mass, and cable cost for the existing AC system under study are:

- Total copper volume: 51.55 m^3
- Total cable mass: 536.23 t
- Total cable cost: 7.26 M€

For the proposed DC minimum-CSA model:

- Total copper volume: 27.01 m^3
- Total cable mass: 298.06 t
- Total cable cost: 4.81 M€

And for the proposed DC constant-J model:

- Total copper volume: 40.19 m^3
- Total cable mass: 418.70 t
- Total cable cost: 5.39 M€

The following assumptions apply to the cost model:

1. Installation and labor costs are excluded.
2. Taxes, transportation, and import duties are not considered.

These simplifications allow the analysis to focus exclusively on the impact of cable sizing and conductor count on material cost.

3.6. Material Usage and Cost Comparison

This subsection summarizes the overall comparison between the AC and DC distribution architectures in terms of total copper volume and cable material and cost, based on the sizing, routing, and redundancy assumptions defined in Sections 3.1 - 3.5.

It should be noted that the pricing adopted for the AC configuration refers to equivalent modern single core low voltage cables currently available on the market. Some cable types used in existing AC installations are no longer considered acceptable under current safety and regulatory standards. Therefore, a commercially available and safety compliant reference has been adopted to ensure a fair and realistic comparison.

Figure 16 presents a normalized comparison between the AC reference system and the proposed DC architectures in terms of copper volume, cable mass, and cable cost. For clarity, the values associated with the AC configuration are taken as the reference and normalized to 100%, while the corresponding DC values are expressed as a percentage of the AC case.

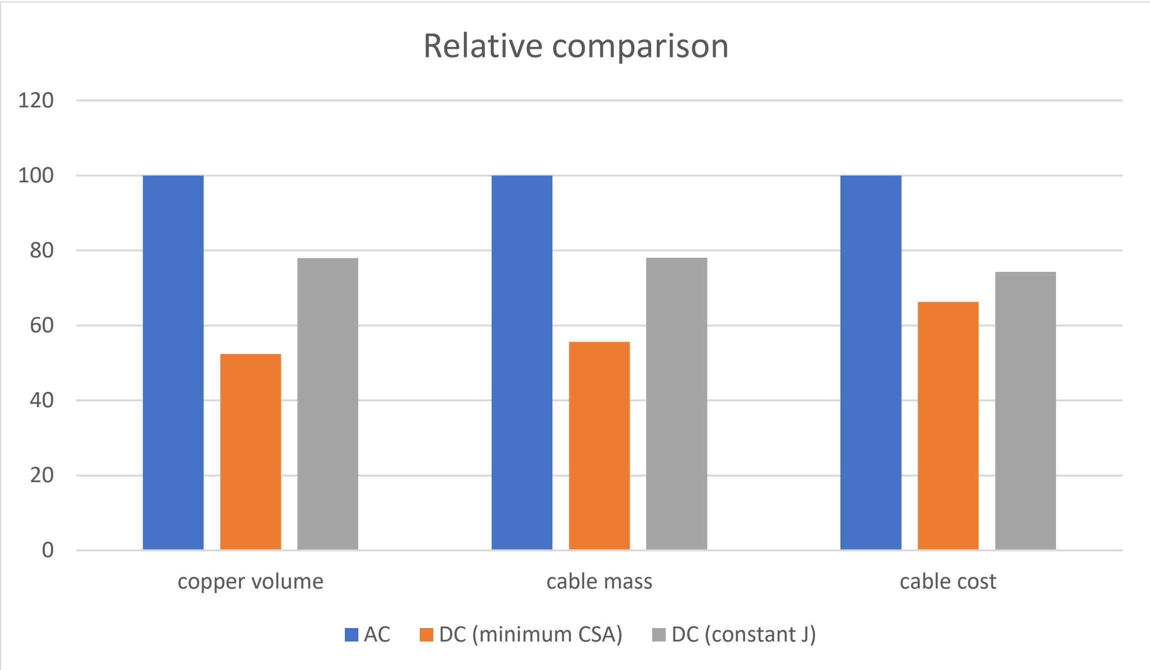

Figure 16. Relative comparison of copper volume, cable mass, and cable cost in AC and DC architecture

Relative to the AC reference, the DC minimum-CSA design yields an estimated 48% reduction in copper volume, 45% reduction in total cable mass, and 34% reduction in cable material cost, under identical topology, load conditions, routing, and redundancy criteria. These reductions are primarily driven by the lower operating currents of the DC architecture, which enable smaller conductor cross-sections, and by the reduced number of current-carrying conductors per circuit.

When the constant-*J* criterion is applied, the DC conductors are intentionally upsized to maintain a current density comparable to the AC reference. As a result, the material savings are reduced compared to the minimum-CSA case, but the DC configuration still maintains a clear advantage over AC in all three metrics. Since the cross-sections selected under the constant-*J* approach are equal to those of the AC design, the associated material saving is only due to reduced number of conductors in the DC system (2 poles instead of 3 phases).

It should be noted that the difference between cable-mass reduction and copper-volume reduction is because copper volume accounts only for conductor material, whereas cable mass also includes insulation and sheath (non-copper) materials that do not scale down proportionally with conductor CSA.

In addition to cable downsizing, the reduced operating currents associated with the DC architecture would also allow a proportional reduction in busbar CSA throughout the distribution system. Smaller busbars would lead to further reductions in copper usage, enclosure size, and thermal stress, contributing to lower material cost and improved spatial efficiency.

Moreover, the proposed DC architecture eliminates the need for downstream isolation transformers that are typically required in the AC configuration. In the reference system, a total of 48 isolation transformers is installed across the distribution chain; removing these units would provide an additional Cap-Ex reduction beyond cable and busbar savings, while also reducing footprint, installation complexity, and transformer-related losses. This effect is not included in the cable material cost comparison of Figure 16 and would further strengthen the economic advantage of the DC solution.

This chapter has quantified the impact of DC distribution on conductor sizing, copper usage, and cable material and cost under identical routing, load, and redundancy assumptions. The results show that the higher operating voltage and reduced number of current carrying conductors in DC architecture led to significantly lower design currents and smaller cable CSAs across all distribution levels. These reductions are achieved without modifying the system topology or reliability assumptions. In addition to technical and economic benefits, the lower copper demand indirectly improves the environmental footprint of the distribution system by reducing raw material extraction, processing, and associated emissions. Furthermore, the reduced conductor size and copper volume also provide secondary advantages in terms of installation space, mechanical handling, and thermal performance, which further motivate the detailed loss and efficiency analysis presented in the following chapter.

4 Power losses, energy losses, and environmental impacts

This chapter quantifies and compares the electrical losses of the AC reference architecture and the proposed DC architecture over a one-year period, with the objective of assessing the potential efficiency improvement achievable through DC distribution. Due to the large volume of operational data involved, the loss analysis is performed using Python scripts. The environmental implications of the calculated annual energy losses, the impact on the system PUE, and electricity cost (Op-Ex) saving are evaluated to better illustrate their practical significance.

In addition to cable losses, power distribution systems include losses associated with busbars at the transformer, UPS, PDU, and RPP levels. These losses are primarily resistive (Joule losses) and follow $P_{\text{bus}} = I^2R$. Therefore, for a given busbar resistance, reduced operating current in the DC architecture would decrease busbar losses quadratically. In this study, busbar losses are not explicitly modeled due to the lack of detailed geometric and material data. However, the reduced operating currents in DC architecture led to lower resistive losses.

Because loss calculations rely on measured operating points, results should be considered with an uncertainty margin to reflect instrumentation tolerance, and modeling approximations. Therefore, the reported annual values should be interpreted as estimates within a reasonable engineering tolerance rather than exact numbers.

To communicate the annual electrical losses in practical terms, the computed annual energy loss is translated into common equivalents:

1. Household equivalents are calculated using ARERA's reference annual household electricity consumption of 2,000 kWh/year [42].
2. Electric Vehicle (EV) driving equivalents are derived using a representative battery electric vehicle consumption range of 0.14 kWh/km to 0.19 kWh/km [43].
3. CO_2 equivalent per kilowatt-hour is estimated using the European Environment Agency (EEA) indicator for the greenhouse gas emission intensity of electricity generation, corresponding to 225 gCO2e/kWh for Italy in 2023 [44]. The detailed values are shown in Figure 17.
4. Tree offset is obtained based on a typical mature tree absorbing around 21 kgCO2/year [45].

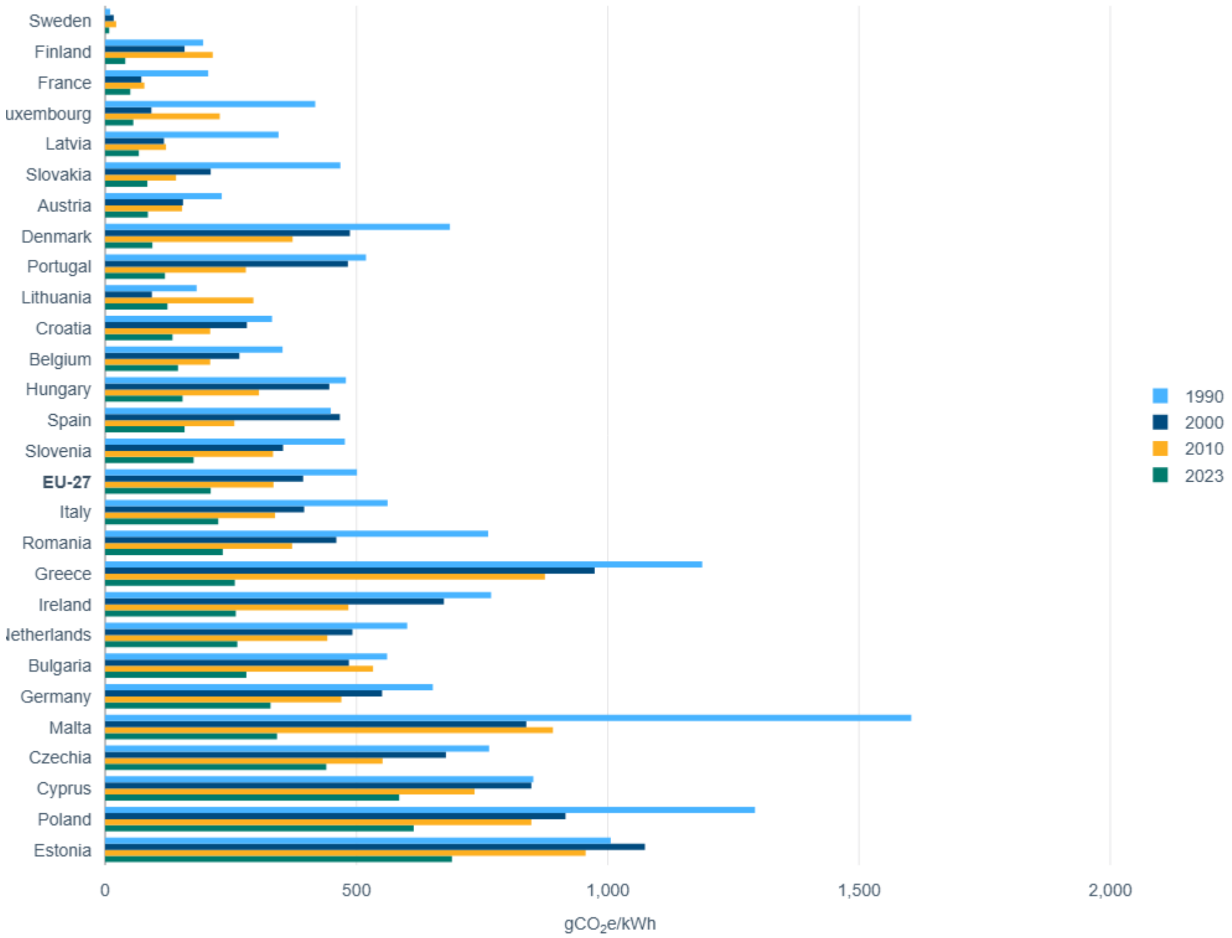

Figure 17. CO2 emission equivalent per kWh for European countries

Figure 17 shows that Italy's electricity generation CO_2 intensity is close to the EU-27 average in 2023. This implies that the emission reductions achieved through improved power distribution efficiency are close to the average in Europe. More generally, the same efficiency improvements would result in different absolute CO_2 savings depending on the country, with larger benefits in regions characterized by higher emission intensities and smaller effects in low carbon systems.

The loss calculations presented in this chapter are based on fundamental frequency RMS currents. Since the system consists of two separate sections (1S and 2S), the results are also divided accordingly.

Losses in the neutral conductor due to load unbalance are also included in the AC analysis. However, additional losses caused by harmonic currents generated by non-linear loads are not explicitly modeled. In practical AC systems, such harmonics can further increase conductor and transformer losses, including additional neutral conductor losses. These effects are not present in DC distribution, which inherently avoids low frequency harmonic currents and neutral conductors, reinforcing the relative efficiency advantage of DC architectures.

4.1. AC losses

Electrical losses in the distribution network are dominated by Joule losses in cables and busbars, which scale with the square of the operating current. To capture the actual operating behavior of the system, losses are evaluated using measured current profiles collected over the year 2024. This time series approach allows the calculation of losses under realistic loading conditions.

4.1.1. Phase Currents Losses

The calculations are based on measured operating data sampled at 15-minute intervals for each phase current across all low voltage distribution lines included in the study.

For each line i, the squared currents for each phase ($I_{A,i}$, $I_{B,i}$, and $I_{C,i}$) are computed at every available timestamp and used to evaluate Joule losses:

$$I_{A,i}{}^2 = \begin{pmatrix} I_{A,i\_1}{}^2 \\ \vdots \\ I_{A,i\_n}{}^2 \end{pmatrix}, \qquad I_{B,i}{}^2 = \begin{pmatrix} I_{B,i\_1}{}^2 \\ \vdots \\ I_{B,i\_n}{}^2 \end{pmatrix}, \qquad I_{C,i}{}^2 = \begin{pmatrix} I_{C,i\_1}{}^2 \\ \vdots \\ I_{C,i\_n}{}^2 \end{pmatrix}$$

As 2024 is a leap year, a complete dataset would consist of $366 \times 24 \times 4 = 35{,}136$ samples per line. In practice, some data points are missing due to measurement or system outages. These gaps are addressed by annualizing the available data, as described later in this section.

The instantaneous power loss of line i at each timestamp is calculated as:

$$P_{loss,i} = R_{i,\theta,L} \times (I_{A,i}{}^2 + I_{B,i}{}^2 + I_{C,i}{}^2)$$

where $R_{i,\theta,L}$ is the total resistance of the line at operating temperature θ and length L.

The resistance at operating temperature is derived from manufacturer data:

$$R_{i,L} = R_i \times L \times 0.001$$

$$R_{i,\theta,L} = R_{i,L}\big(1 + \alpha(\theta - 20)\big)$$

where R_i is the resistance per unit length at 20 °C (Ω/km), L is the line length in meters, $\alpha = 0.004\ °\mathrm{C}^{-1}$ is the temperature coefficient of resistance, and the conductor temperature is assumed equal to 75 °C for downstream cables and 70 °C for upstream cables.

It should be noted that, the conductor resistance values adopted in this analysis are based on standard tabulated DC resistance data corrected for operating temperature. At power frequency (50 Hz), AC conductors exhibit a slight increase in effective resistance due to skin and proximity effects, which cause current redistribution within the conductor CSA and among adjacent conductors. For the low-voltage copper cable sizes considered in this study, this increase remains limited and is commonly neglected in practical engineering calculations. This assumption slightly underestimates the actual resistive losses in the AC configuration. As a result, the calculated efficiency advantage of DC architecture can be considered conservative, and the real performance gap between AC and DC distribution may be marginally larger than reported.

For each line, four loss indicators are then calculated:

- Sum of power loss samples [MW]:

$$P_{i,\text{data}} = \frac{\sum_{data} P_{loss,i}}{10^6}$$

- Estimated sum of power losses [MW]:

$$P_{i,\text{total}} = P_{i,\text{data}} \times \frac{35{,}136}{N_{\text{data},i}}$$

where $N_{\text{data},i}$is the number of valid samples available for line i.

- Total annual energy loss [MWh]:

$$E_{i,\text{total}} = P_{i,\text{total}} \times 0.25$$

- Average power loss [kW]:

$$P_{i,\text{av}} = \frac{E_{i,\text{total}}}{8784} \times 1000$$

Finally, the losses are aggregated across all lines belonging to each system level.

For the isolation transformer, the input and output active powers are obtained from measurements, and their difference is used to estimate transformer losses:

$$P_{trans} = P_{trans,in} - P_{trans,out}$$

The resulting power and energy losses for the AC configuration are summarized in Table 4.

This methodology ensures that variations in load, utilization, and operating conditions are directly reflected in the loss evaluation, rather than relying on nominal or peak current assumptions.

Table 4. Power loss and energy loss for the AC configuration in 2024

Levels	Sum of power loss samples [MW]	Estimated sum of power losses [MW]	Total energy loss [MWh]	Average power Loss [kW]
1S-RPP level	1664	1705	426.3	48.53
2S-RPP level	2299	2333	583.3	66.40
1S-PDU level	619.5	628.7	157.2	17.89
2S-PDU level	564.9	572.97	143.2	16.31
1S-UDP level	232	235.5	58.9	6.70
2S-UDP level	194.4	197.2	49.3	5.61
1S-transformer	3212	3259.5	814.9	92.77
2S transformer	3747.4	3802.8	950.7	108.23
Total	**12533.9**	**12734.9**	**3183.7**	**362.44**

The total annual energy loss of approximately 3.18 GWh corresponds to an average continuous dissipation of 362 kW. From an operational perspective, this thermal load must be continuously removed by the cooling infrastructure. This results in additional indirect energy consumption.

4.1.2. Unbalanced Load Losses

In addition to phase conductor losses, the impact of load imbalance is evaluated by estimating the neutral current downstream of the PDU bus. Upstream feeders are supplied from the grid and are assumed to operate with balanced three phase currents; therefore, neutral losses are only considered for the final low voltage feeders where single phase load allocation can create current imbalance.

For each line and each 15-minute timestamp, the phase currents are first checked against a balance criterion using phase A as the reference:

$$|I_B - I_A| \leq 0.1\,|I_A|$$
$$|I_C - I_A| \leq 0.1\,|I_A|$$

A 10% tolerance is adopted to account for measurement uncertainty. When either inequality is violated, the currents are treated as unbalanced, and the resulting negative/zero-sequence component is used to estimate the neutral current magnitude. Using a symmetrical component formulation, the imbalance current is computed as:

$$I_{\text{imb, real}} = I_A - \frac{I_B + I_C}{2}$$
$$I_{\text{imb, img}} = \frac{\sqrt{3}}{2}(I_B - I_C)$$
$$I_{\text{imb}} = \sqrt{I_{\text{imb,real}}^2 + I_{\text{imb,img}}^2}$$

The neutral-current magnitude is then taken as $I_{N,i} = I_{\text{imb}}$ for the corresponding timestamp, and the instantaneous neutral Joule loss is calculated like the phase-loss computation:

$$P_{\text{loss},i} = R_{i,\theta,L}\, I_{N,i}^2$$

The same annualization approach used for phase losses is applied to obtain the estimated annual power loss, total annual energy loss, and average power loss for the neutral conductor. The aggregated results are reported in Table 5.

Table 5. N line losses due to unbalanced load

Levels	Sum of power loss samples [MW]	Estimated sum of power losses [MW]	Total energy loss [MWh]	Average power Loss [kW]
1S unbalanced losses	286	293	73.2	8.34
2S unbalanced losses	84.0	85.2	21.3	2.42
total	370	378.2	94.5	10.76

The neutral losses amount to approximately 94.5 MWh over 2024, corresponding to an average dissipation of 10.76 kW. This is about 3% of the phase-conductor losses and is therefore relatively small; however, it is retained in the AC loss budget for completeness. In addition, since this imbalance is not present in a bipolar ±400 V DC system where all the loads are considered 800V, adding the N line losses in AC helps in comparing AC and DC more realistically.

4.1.3. Total AC Losses

The total electrical losses of the AC distribution network are obtained by summing the phase-conductor losses (Table 4) and the neutral losses due to unbalance (Table 5). Therefore:

$$E_{\text{AC,total}} = E_{\text{phase,total}} + E_{\text{neutral,total}}$$
$$P_{\text{AC,av}} = P_{\text{phase,av}} + P_{\text{neutral,av}}$$

Using the aggregated values reported previously:

- Total AC energy loss:
$$E_{\text{AC,total}} = 3183.7 + 94.5 = 3278.2\ \text{MWh}$$

- Average AC power loss:
$$P_{\text{AC,av}} = 362.44 + 10.76 = 373.2\ \text{kW}$$

These values represent the overall annual dissipation associated with the AC distribution conductors (phases and neutral) under the measured 2024 operating profile.

4.2. DC Losses with Minimum Possible CSA

This section evaluates the electrical losses of the DC distribution architecture sized with the minimum conductor CSA allowed by the ampacity and voltage drop constraints defined in Chapter 3.

The analysis is based on measured operating data from 2024. For each distribution line i, the measured active power profile is extracted. Since the IT load is assumed to be identical for the AC and DC architectures, the instantaneous DC current is derived from the measured power as:

$$I_i = \frac{P_i}{V_{DC}} = \begin{pmatrix} P_{i,1} \\ \vdots \\ P_{i,n} \end{pmatrix} \times \frac{1}{800}$$

The instantaneous power loss of line i is then evaluated as:

$$I_i^{\,2} = \begin{pmatrix} I_{i,1}^{\,2} \\ \vdots \\ I_{i,n}^{\,2} \end{pmatrix}$$

$$P_{loss,i} = 2 \times R_{i,\theta,L} \times (I_i^{\,2})$$

The factor of 2 accounts for the bipolar ±400 V DC configuration, in which current flows through both the positive and negative conductors. The line resistance $R_{i,\theta,L}$ is calculated using the same temperature-correction methodology adopted for the AC case, ensuring consistency between configurations.

As in Section 4.1, the following loss indicators are calculated for each line:

- Sum of power loss samples [MW]:

$$P_{i,\text{data}} = \frac{\sum_{data} P_{loss,i}}{10^6}$$

- Estimated sum of power losses [MW]:

$$P_{i,\text{total}} = P_{i,\text{data}} \cdot \frac{35{,}136}{N_{\text{data},i}}$$

- Total annual energy loss [MWh]:

$$E_{i,\text{total}} = P_{i,\text{total}} \cdot 0.25$$

- Average power loss [kW]:

$$P_{i,\text{av}} = \frac{E_{i,\text{total}}}{8784} \times 1000$$

Losses are then aggregated across all lines belonging to each system level. The resulting power and energy losses for the DC configuration with minimum CSA are summarized in Table 6.

Table 6. Energy and power losses for DC architecture with minimum CSA

Levels	Sum of power loss samples [MW]	Estimated sum of power losses [MW]	Total energy loss [MWh]	Average power loss [kW]
1S RPP level	1143.4	1173.4	293.4	33.4
2S RPP level	1595.4	1618.7	404.7	46.1
1S PDU level	608.3	617.7	154.4	17.5
2S PDU level	561.79	569.7	142.4	16.2
1S UDP level	228.1	231.7	57.9	6.6
2S UDP level	192	195	48.8	5.6
1S transformer	0	0	0	0
2S transformer	0	0	0	0
Total	4329	4406.4	1101.6	125.4

The results indicate that DC losses are consistently lower than AC losses at all distribution levels. In addition, the elimination of the isolation transformer in the DC architecture results in zero transformer level losses, contributing significantly to the overall reduction in power dissipation. The total annual energy loss is reduced to approximately 1.10 GWh, corresponding to an average continuous dissipation of 125 kW, which represents a reduction of more than 66% compared to the AC reference case.

4.3. DC losses with similar current density as AC

In this section, the DC conductors are sized to match the current density of the existing AC configuration.

The current density J is defined as:

$$J = \frac{I_{\ell,worst}}{CSA}$$

where $I_{\ell,\mathrm{worst}}$ is the worst-case line current at level ℓ, and CSA is the conductor CSA.

Based on the AC configuration analyzed in Chapter 3, representative current density values are obtained for different system levels. Values of approximately 1.57 A/mm² and 1.52 A/mm² are observed for the UPS input and output feeders, respectively, while values of 1.27 A/mm² for PDU, and 1.16 A/mm² for RPP are obtained.

Forcing the same current density for the DC configuration, the required CSA is calculated as:

$$CSA = \frac{I_{\ell,worst,DC}}{J}$$

Applying this relation leads to the following indicative DC conductor sizes:

- UPS input and output feeders: $CSA \approx 197\ \mathrm{mm}^2$
- PDU level feeders: $CSA \approx 197\ \mathrm{mm}^2$
- RPP level branches: $CSA \approx 58\ \mathrm{mm}^2$

Referring to the DC ampacity tables, the closest available standard conductor sizes are therefore selected as:

- 240 mm² for UDP and PDU level feeders,
- 70 mm² for RPP level branches.

These values coincide with the conductor sizes currently used in the AC architecture.

With these conductor sizes, the DC losses are calculated following the same methodology adopted in Section 4.2. The resulting power and energy losses are summarized in Table 7.

Table 7. Energy and power losses for DC architecture with constant current density

Levels	Sum of power loss samples [MW]	Estimated sum of power losses [MW]	Total energy loss [MWh]	Average power loss [kW]
1S RPP level	805.75	826.87	206.7	23.53
2S RPP level	1124.25	1140.69	285.2	32.46
1S PDU level	302.6	307.3	76.8	8.75
2S PDU level	280.89	284.88	71.2	8.11
1S UDP level	114	115.86	29.0	3.30
2S UDP level	96	97.5	24.4	2.78
1S transformer	0	0	0	0
2S transformer	0	0	0	0
Total	**2723.6**	**2773**	**693.3**	**78.93**

The total annual energy loss in this scenario is approximately 0.69 GWh, corresponding to an average continuous dissipation of 78.9 kW. Compared to the minimum CSA DC configuration analyzed in Section 4.2, losses are further reduced due to the increased conductor CSAs. This case represents a conservative DC design that preserves AC-equivalent thermal margins while still benefiting from the higher operating voltage and the elimination of AC-specific conversion stages. In this scenario, the same cables could be kept, if the existing cables are suitable for DC operation at the required voltage.

Compared to the AC reference case, this represents a reduction of about 79% in annual energy losses. This result indicates that a conservative DC design, while maintaining AC-equivalent thermal margins, can significantly improve operational efficiency and environmental impact.

4.4. Power Losses Comparison

This section compares the AC reference architecture with the two DC configurations using the most representative performance indicators: total annual energy loss and average power loss. A summary of the results is presented in Table 8, while Figure 18 and Figure 19 illustrate the comparison graphically.

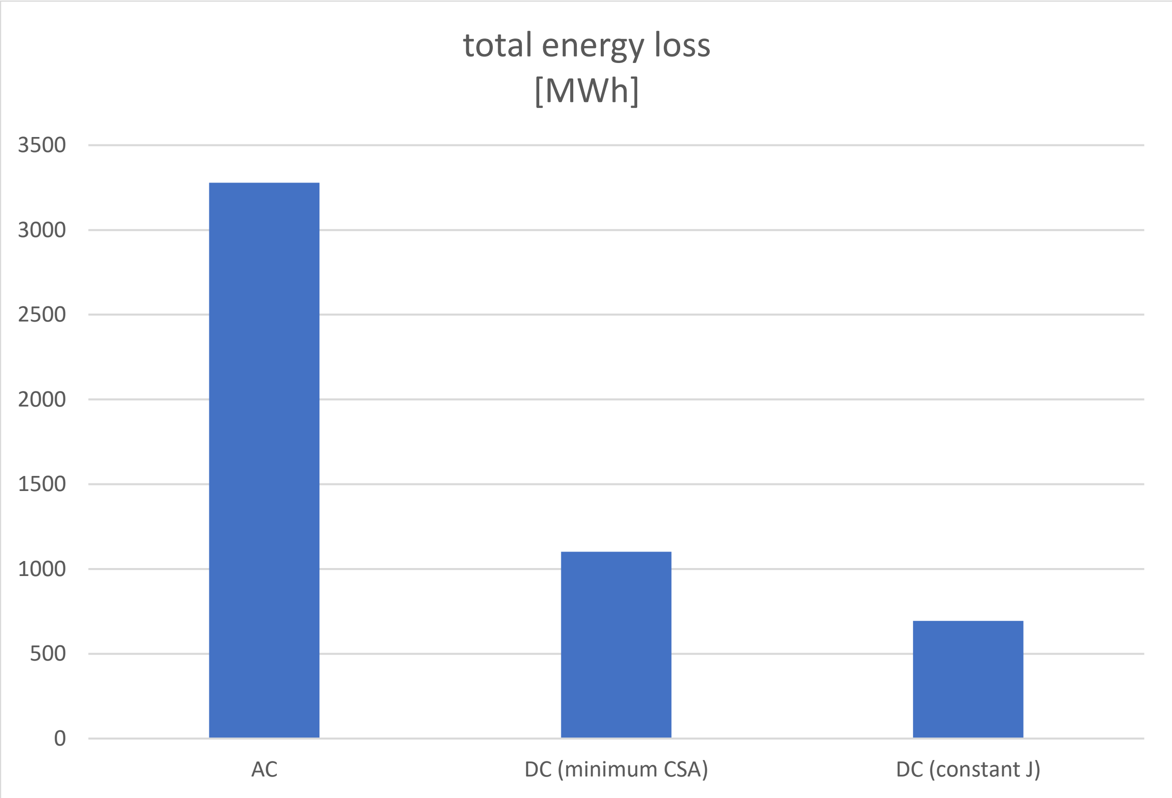

Figure 18. Total energy loss comparison

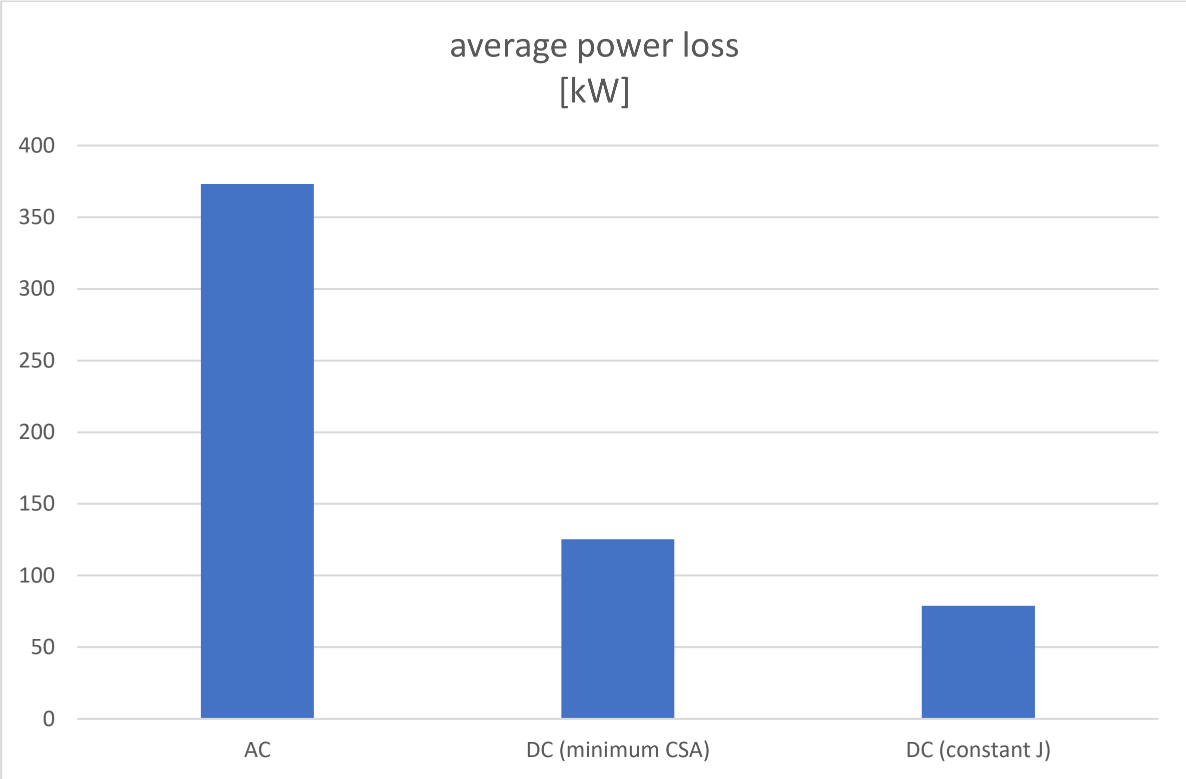

Figure 19. Average power loss comparison

Table 8. Energy and power loss comparison

Configuration	Total energy loss [MWh]	Average power loss [kW]
AC	3278	373.2
DC - minimum CSA	1102	125.4
DC - constant J	693	78.93

The results show a substantial reduction in electrical losses when transitioning from the AC architecture to DC distribution.

In the DC configuration with minimum conductor CSA, annual losses decrease to 1102 MWh and 125.40 kW, representing a reduction of approximately 66% relative to the AC case. This configuration benefits from lower operating currents, and the elimination of the isolation transformer, while also minimizing copper usage. However, losses remain higher than in a more conservatively sized DC design.

When the DC conductors are sized to maintain the same current density as the AC configuration, total annual losses further decrease to 693 MWh, with an average power loss of 78.93 kW. This corresponds to an overall reduction of approximately 79% compared to the AC system and about 37% relative to the DC minimum-CSA case, confirming that optimized conductor sizing is highly effective in reducing I^2R losses.

Overall, both DC configurations significantly outperform the AC architecture. The minimum CSA solution prioritizes reduced copper usage and material cost, while the constant current density solution achieves the lowest electrical losses and represents a conservative, thermally robust design.

This chapter has demonstrated that DC distribution significantly reduces electrical losses compared to the conventional AC architecture when evaluated under identical load profiles and operating conditions. These improvements are attributed to lower operating currents, and the elimination of isolation transformer stage. The results also show that conductor sizing represents a key design lever: while the minimum-CSA solution prioritizes material savings, a more conservative sizing approach can substantially enhance energy efficiency. Overall, the loss analysis confirms that DC distribution offers both operational and economic advantages over AC systems, with both reducing electricity usage and eliminating isolation transformers, providing a strong basis for the environmental and efficiency considerations discussed in the following sections.

4.4.1. Energy saving price

Based on the data given by the company, the average energy price for the year 2024 is 181 €/MWh. Therefore, the price for total energy loss for each case is calculated and tabled in Table 9, and visualized in Figure 20.

Table 9. Total energy loss price comparison

Configuration	Annual energy loss cost [k€]
AC	593.4
DC - minimum CSA	199.5
DC - constant J	125.4

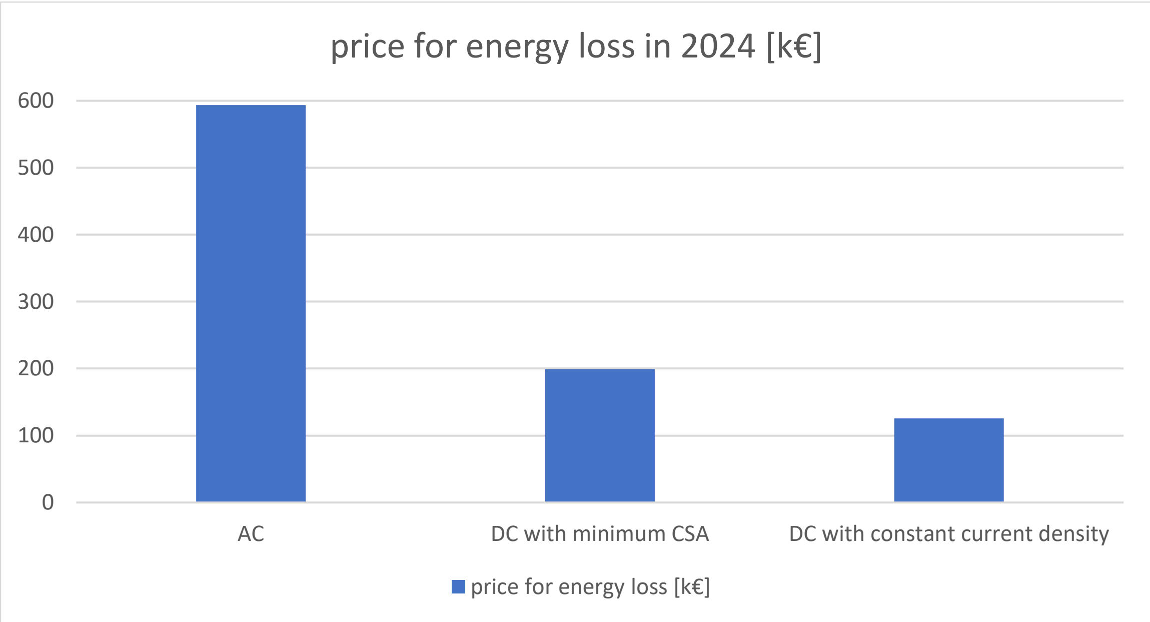

Figure 20. Total energy loss price comparison

The comparison of annual energy loss costs highlights a substantial economic advantage of the DC-based distribution architectures over the conventional AC configuration. The AC system results in a total annual energy loss cost of 593.4 k€, whereas the DC configuration designed with minimum conductor cross-sectional area (CSA) reduces this value to 199.5 k€, corresponding to an annual saving of 393.9 k€. An even greater reduction is achieved with the DC architecture designed under a constant current density criterion, which yields annual energy losses cost of 125.4 k€. Compared to the AC system, this represents a yearly saving of 468 k€, equivalent to a reduction of approximately 79%. These results clearly demonstrate that, over a single year of operation, DC distribution architectures can deliver significant cost savings by minimizing conduction losses, with the constant current density design providing the most efficient solution among the configurations analyzed.

4.4.2. Environmental impacts

To provide a better view of the calculated electrical losses, the annual energy losses of the three configurations are translated into environmental equivalents. These indicators do not represent precise estimates but are intended to communicate the relative magnitude of losses in familiar terms.

- For the AC reference configuration, the annual energy loss of 3278 MWh corresponds to the electricity consumption of approximately 1640 households, roughly 17 - 23 million kilometers of EV driving, and about 738 t of CO_2 emissions per year, which would require on the order of 35 thousand mature trees to offset.
- In the DC configuration with minimum conductor cross-sectional area, the annual energy loss decreases to 1100 MWh. This corresponds to approximately 550 households, 6 - 8 million kilometers of EV driving, and about 248 t of CO_2 emissions per year, equivalent to roughly 11.8 thousand trees to offset.
- The DC configuration with constant current density exhibits the lowest environmental impact. With annual losses of 693 MWh, the equivalent impact is reduced to about 350 households, 3.5 - 5 million kilometers of EV driving, and approximately 156 t of CO_2 emissions per year, corresponding to roughly 7400 trees.

Figure 21. Environmental benefits of DC with respect to AC architecture

Figure 21 shows a visualized approximation of environmental benefits of the DC (both minimum CSA and constant J approaches) architecture with respect to AC model.

The environmental indicators presented in this section provide an intuitive interpretation of the calculated electrical losses and their broader implications. Household equivalents, EV-driving distances, and tree-offset metrics are provided as communication metrics to show the relative scale of energy losses in intuitive terms. They do not represent a formal environmental impact assessment, which would require a full life cycle analysis and specific emission factors. Therefore, they should be interpreted as comparative and illustrative tools, rather than as absolute metrics.

Nevertheless, these metrics effectively illustrate the relative magnitude of losses associated with each architecture. The results show that both DC configurations lead to substantial reductions in energy related emissions, with the constant current density design achieving nearly an 80% reduction compared to the AC reference system. These findings reinforce the conclusion that DC distribution can play a meaningful role in improving the sustainability of hyperscale data centers.

4.4.3. Effects on Power Usage Effectiveness

In this subsection, the impact on Power Usage Effectiveness (PUE) is evaluated by considering only the variation in electrical distribution losses within the facility boundary. Electrical losses associated with power conversion, transformers, UPS systems, and distribution cables are treated as part of non-IT energy consumption. The interaction between reduced electrical losses and cooling energy demand is not explicitly modeled. Therefore, the reported PUE variation represents a first order, indicative assessment of the effect of reduced electrical losses, rather than a fully coupled electrothermal facility model.

PUE is defined as:

$$PUE = \frac{Total\ Facility\ Energy}{IT\ Equipment\ Energy}$$

Assuming a nominal PUE of 1.35 for the AC reference case and an IT load of 9.6 MW, the corresponding non-IT overhead power is approximately 3.36 MW.

Under a first-order approximation, where reduced distribution losses directly reduce overhead power, the DC minimum-CSA configuration would lower overhead demand by about 0.24 MW, yielding an estimated PUE of approximately 1.324. For the DC constant current density configuration, the overhead reduction is about 0.28 MW, corresponding to an estimated PUE of approximately 1.320.

While these values represent simplified estimates and do not account for secondary effects (e.g., cooling efficiency changes), they indicate that loss reductions in the distribution level alone can contribute a measurable improvement in overall data center energy efficiency.

5 Availability and Reliability

This chapter evaluates the availability and reliability performance of the AC and DC distribution architectures using the Reliability Block Diagram (RBD) method, implemented in Python. RBDs are a well-established and widely used approach for modeling complex power systems, as they allow the representation of series, parallel, and redundant configurations in a transparent and mathematically tractable manner.

The distinction between availability and reliability can be clarified through a simple example. A component that fails very rarely but requires a long repair time may exhibit high reliability over a given mission time but relatively low availability. Conversely, a component that fails more frequently but can be restored quickly may achieve high availability while still having lower reliability over long operation periods.

In data center applications, both metrics are essential, as availability reflects service continuity under repairable failures, while reliability captures the probability of uninterrupted operation over extended time horizons.

5.1. Methodology and metrics

Component reliability data are extracted from the IEEE Std. 493-2007 (Gold Book), which provides standardized Mean Time Between Failures (MTBF) and Mean Time to Repair (MTTR) values for electrical power system components. The derivation assumes independent components; each system component is modeled as a reliability block, and the overall system behavior is obtained by combining these blocks according to the system topology.

Both availability and reliability are evaluated in this study:

- Availability (A) is defined as the fraction of time the system is operational, accounting for both failures and repairs. It depends on MTBF and MTTR.
- Reliability (R) is defined as the probability that the system operates without failure over a specified time interval [0, t]. It depends on MTBF and the assumed distribution of failures.

An exponential failure distribution is adopted for all components, which is commonly used for comparative reliability studies.

5.2. Modeling approach and assumptions

To reflect the structure, the system is modeled by separating the upstream and downstream sections. The availability and reliability of each section are calculated independently and then combined in series. This approach improves model clarity and allows a direct comparison between architectures.

The analysis is based on the following assumptions:

- All components upstream of the MV/LV transformers are considered relatively reliable, with MTBF = 10^9 hours and MTTR = 0, resulting in $A \approx 1$ and $R \approx 1$.
- The analysis includes Circuit Breakers (CBs) , bus ducts, cables, transformers, batteries, rectifiers, and inverters.
- Components for which no data is available (e.g. cable connections and auxiliaries) are excluded from the model.
- Due to lack of detailed information, all components downstream of the RPP bus, except for the rectifier, are excluded.
- All IT loads are assumed to operate at 800 V DC in the DC architecture.
- In the AC architecture, the battery system consists of five parallel strings with N+1 redundancy.
- In DC architecture, two identical battery systems (the same as the one considered for AC) are modeled in series for reliability modeling purposes, to represent the 800 V DC supply; this does not imply a physical series connection.

Because the analysis relies on standardized data and idealized assumptions, the resulting availability and reliability values should be interpreted as comparative indicators, not as exact predictions of field performance.

5.3. Structures and data

The following structures are used:

- Series structure (AND logic): all components must operate for the system to function.
- Parallel structure (OR logic**):** the system operates if at least one component operates.
- k-out-of-n (k-oo-n) structure: the system operates if at least k components out of n components are operational.

These structures are combined to model the system.

The components used for AC and DC models are represented in Table 10 and Table 11, respectively.

Table 10. AC components

Component	IEEE Category	MTBF [h]	MTTR [h]
Circuit breaker (n.o., n.c.)	E12-211 / E12-212	5.6×10^7 / 7.8×10^7	0 / 18.67
Bus duct	E3-000	2.88×10^7	0
Cable	E6-111	1.29×10^7	8
Transformer	E38-113	1.44×10^7	0
Battery	E2-120	1.17×10^6	32.13
Rectifier	E32-000	1.96×10^6	16
Inverter	E25-000	1.82×10^6	26

Table 11. DC components

Component	IEEE Category	MTBF [h]	MTTR [h]
DC switch	E34-221	1.38×10^7	0
Bus duct	E3-000	2.88×10^7	0
DC cable	E8-100	1.20×10^6	2
Transformer	E38-113	1.44×10^7	0
Battery	E2-120	1.17×10^6	32.13
Rectifier	E32-000	1.96×10^6	16

Note: MTBF and restoration/repair times are taken directly from IEEE Std 493. Some entries report a restoration time of 0 h. In the standard dataset this can represent cases where repair time is negligible compared to the mission time, not explicitly modeled, or handled as a replacement/non-repairable assumption. In this thesis, these values are used consistently for both architectures to support a relative comparison rather than a site-specific downtime prediction.

5.4. Analyzed configurations

Two reliability and availability analyses are performed:

a) System-level analysis: The upstream is considered with 3-to-make-2 redundancy (2oo3) and downstream with 2N redundancy (1oo2). This case represents the reliability of the entire power distribution infrastructure. Which denotes if the system can feed all the loads.

b) Load-level analysis: Both upstream and downstream sections are modeled, and both are considered as 2N redundancy and combined in series. This case reflects the reliability from the perspective of an individual load, which is supplied by only two independent paths and does not benefit from the third upstream path. This case shows if a specific load is fed without failure.

In both cases, the model is divided into two separate sections to simplify the system-level and load-level analysis:

1. Grid to PDU bus: including every component in the upstream MV system, MV/LV transformers, UPS system and bypass, UDP, and PDU bus
2. PDU panel to rack: including the CBs, cables, and RPP bus.

The AC architecture also includes the final rectifier stage inside the rack to ensure consistency with the DC supply structure. While in DC, both the UPS path and UPS bypass include a rectifier after the MV/LV transformer to change the system from AC to DC. The RBD structures of AC upstream, DC upstream, and downstream models are shown in Figure 22, Figure 23, and Figure 24, respectively.

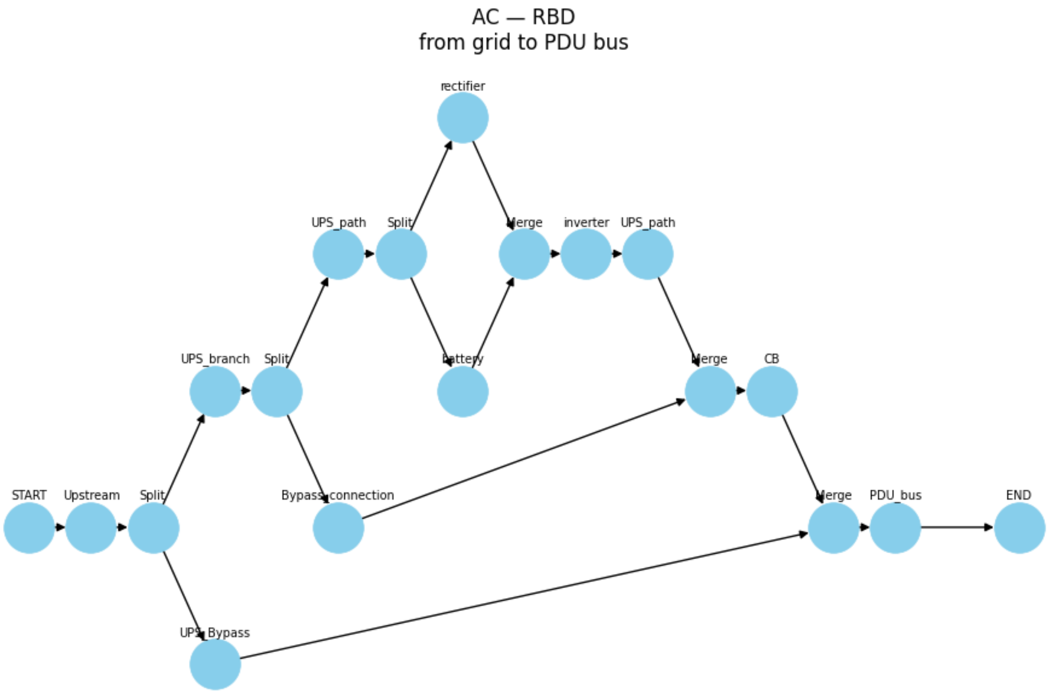

Figure 22. AC Block diagram: from grid to PDU

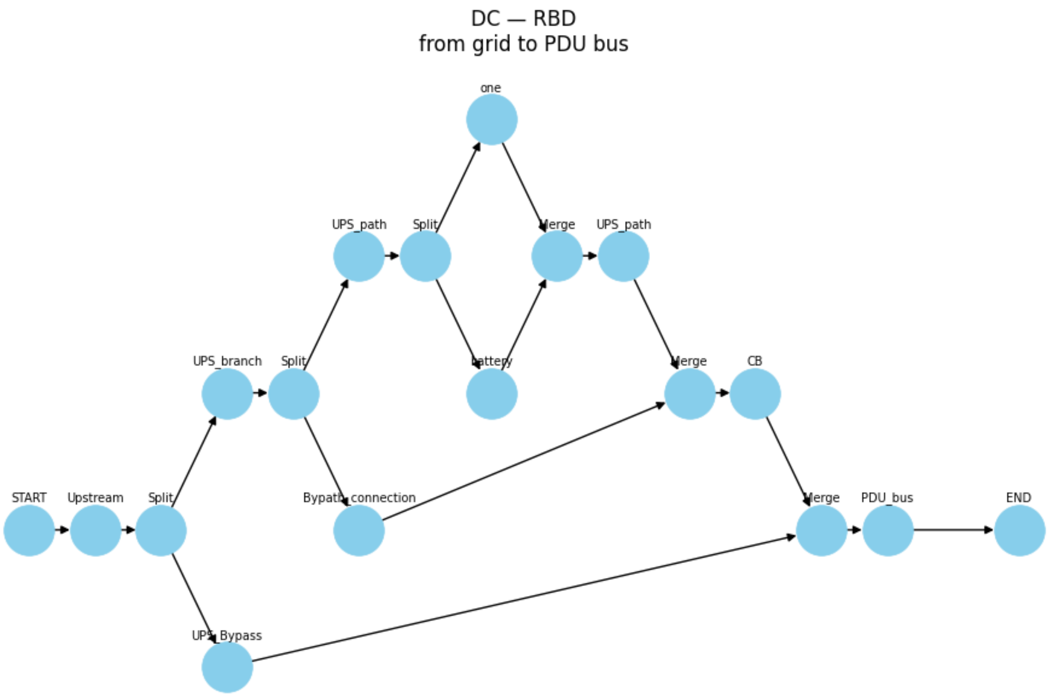

Figure 23. DC block diagram: from the grid to PDU

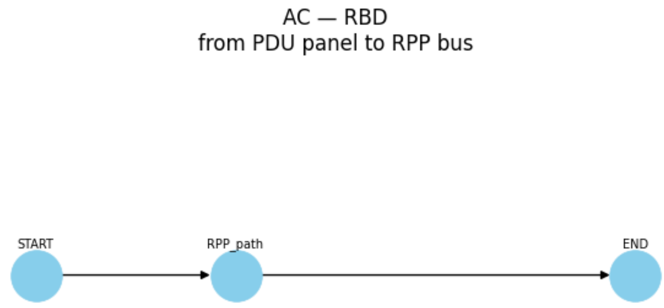

Figure 24. AC and DC block diagram: from PDU to RPP

It should be noted that, although the parameters of AC and DC components differ, the overall system structure of the AC and DC architectures is similar downstream. Therefore, Figure 24 can be considered representative of both AC and DC models.

In Figure 22, the UPS is modeled as a battery connected in parallel with the rectifier and then in series with an inverter. This configuration reflects the operational behavior of the UPS: if the UPS feeder fails, the battery can supply the load; if the battery fails, the upstream source can still feed the load through the rectifier; however, if the inverter fails, the entire UPS path is unable to provide power to the load.

On the other hand, Figure 23, which refers to the DC system upstream, shows the battery connected in parallel with a component that has unity reliability and availability, and no inverter is present. This represents a significant advantage of DC architecture. In this case, if the battery fails, the upstream DC source can continue to supply the downstream loads without interruption. Moreover, since both the system and the battery operate in DC, an inverter is not required, resulting in a simpler and more reliable power path.

5.5. Availability

Availability represents the fraction of time a component is operational, accounting for both failure occurrence and repair processes. Under the assumption of constant failure and repair rates, the steady-state availability of a single component can be expressed as a function of its Mean Time Between Failures (MTBF) and Mean Time to Repair (MTTR).

For a single component, availability is calculated as:

$$A = \frac{MTBF}{MTBF + MTTR}$$

Redundant power distribution architectures are commonly represented using k-out-of-n (k-oo-n) models. Assuming statistically independent and identical components, the combined availability can be derived by summing the probability of all operational states satisfying the k-out-of-n condition.

For a k-out-of-n configuration composed of identical components, the combined availability is given by:

$$A_{koon} = \sum_{i=k}^{n} \binom{n}{i} A^i (1 - A)^{n-i}$$

Where:

- $\binom{n}{i} = \frac{n!}{i!(n-i)!}$
- A = availability of one component

This formulation is used throughout the study to model 2oo3 and redundancy schemes in a consistent and comparable manner.

Applying this general formulation to the redundancy schemes considered in this study yields:

$$A_{2oo3} = 3A^2 - 2A^3$$

For parallel components, availability is calculated as:

$$A_{parallel} = 1 - \prod_i (1 - A_i)$$

while for series components the availability is:

$$A_{series} = \prod_i A_i$$

As described in Section 5.4, two availability metrics are evaluated:

- System availability (A_{system}): the probability that the overall power distribution system is operational at a given time, accounting for failures and repairs.
- Load availability (A_{load}): the probability that an individual load is energized at an arbitrary time.

Based on the final availability A_{system}/A_{load} of the system, the Unavailability (U) and downtime (D) can also be calculated:

$$U = 1 - A$$

$$D = U \times 8760$$

Unavailability (U) represents the fraction of time during which the system or load is not operational. It is the complement of availability and indicates the probability that the system is in a failed state at an arbitrary time. Downtime (D) expresses this unavailability in terms of time and represents the expected total number of hours per year during which the system or load is not available for operation; and 8760 represents the total hours present in a year.

Using generic data from IEEE Std 493 and assuming constant repair times, the RBD analysis results in a system availability of 0.9999918 for the AC architecture and 0.999999999999 for the proposed DC architecture.

It should be noted that availability values beyond approximately five to six nines exceed the practical resolution that can be justified using generic MTBF/MTTR data and constant rate assumption. Therefore, in this section the results are primarily used as comparative indicators to assess the relative impact of architectural choices under consistent assumptions, rather than as absolute predictions of uptime or downtime.

Although availability values beyond five nines exceed the practical resolution, the comparison remains meaningful. Under identical modeling assumptions, the results indicate several orders of magnitude reduction in unavailability for DC architecture, reflecting the higher structural robustness of the DC topology and the reduced number of critical conversion stages. Detailed availability results and comparisons are discussed in Section 5.7.

5.6. Reliability

Reliability is evaluated assuming an exponential failure distribution for all components. Under this assumption, the reliability of a single component over a mission time t is expressed as:

$$R = e^{-\frac{t}{MTBF}}$$

The mission time is set to five years, corresponding to $t = 43800$ h.

For a k-out-of-n configuration composed of identical components, the combined reliability is given by:

$$R_{koon}(t) = \sum_{i=k}^{n} \binom{n}{i} R(t)^i (1 - R(t))^{n-i}$$

For parallel components, reliability is calculated as:

$$R_{parallel}(t) = 1 - \prod_i (1 - R_i(t))$$

For series components the reliability is:

$$R_{series}(t) = \prod_i R_i(t)$$

Consistently with the analysis of availability, two reliability metrics are evaluated:

- System reliability (R_{system}): the probability that the entire power distribution system performs its required function without failure over the mission time t.
- Load reliability (R_{load}): the probability that an individual load receives uninterrupted power over the same mission time.

Using the RBD approach and the adopted mission time, the analysis yields a system reliability of 0.9766 for the AC architecture and 0.9970 for the proposed DC architecture. These values correspond to a reduction in the probability of system failure over five years from approximately 2.34% in the AC case to 0.30% in the DC case, i.e., a failure probability more than seven times lower under identical modeling assumptions.

While absolute reliability values are influenced using general component data and simplified failure models, the relative comparison remains meaningful. The results indicate that DC architecture provides a higher probability of uninterrupted operation over long mission times, mainly due to its reduced number of critical conversion stages and simplified power flow structure. A more detailed comparison of system-level and load-level reliability is presented in the following section.

5.7. Results and comparison

This section compares the AC-based and DC-based power distribution architectures in terms of availability and reliability, evaluated at both system level and load level. The results are summarized in Table 11 and Table 12, and the main differences are discussed in the following subsections.

5.7.1. Availability comparison

From the availability analysis, both architectures exhibit very high steady-state availability; however, the DC architecture consistently outperforms the AC architecture.

Table 12. Availability comparison

Configuration	Level	Availability	A_{system}	A_{load}
AC	Grid -> PDU	0.99999292458500	0.9999918367844	0.9999918368845
	PDU -> rack	0.99999999999999		
	Rectifier	0.99999183693460		
DC	grid -> PDU	0.99999949338720	0.9999999999991	0.9999999999996
	PDU -> rack	0.99999999999993		

In Table 12, values are reported with full numerical precision from the computation; however, consistent with Section 5.5, differences beyond approximately five to six nines should be interpreted only as order of magnitude indicators of unavailability.

This improvement corresponds to a reduction in expected downtime by several orders of magnitude for the DC system. The primary reason is the reduced number of conversion stages and active components in DC architecture. In particular, the elimination of the rack level rectifier and its relocation to an upstream position result in a single rectifier serving multiple racks per path, thereby reducing the number of components connected in series. Since each additional series component increases unavailability, even when individual component availability is very high, this architectural simplification has a significant impact.

A similar trend is observed at load level. The difference between system-level and load-level availability is relatively small in both architectures, as components upstream of the MV/LV transformer are assumed relatively reliable in both cases. Nevertheless, DC architecture benefits more strongly from redundancy and architectural simplicity, resulting in availability values approaching the ideal limit.

For a clearer view of the calculated availability, the corresponding equivalent downtime values are presented in Figure 25. The vertical axis represents the downtime in seconds and is shown on a logarithmic scale.

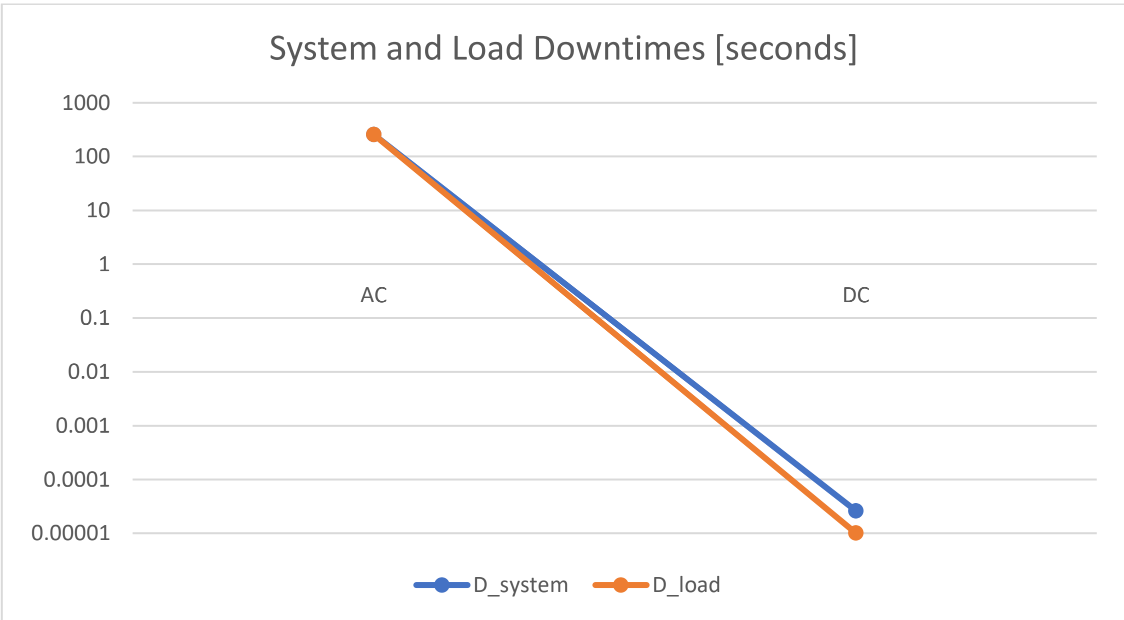

Figure 25. AC vs DC Downtimes

As observed, the equivalent downtime derived from the availability model decreases from hundreds of seconds per year to less than 1 second per year for the proposed DC architecture. It should be noted that actual downtime in real operating conditions may differ, as it is also influenced by additional factors such as fault detection, restoration procedures, and operational practices.

5.7.2. Reliability comparison

In addition to availability, reliability evaluated over the five-year mission time highlights significant differences between the two architectures. The DC system shows a higher probability of uninterrupted operation over the 5 years as shown in Table 13.

Table 13. Reliability comparison

Configuration	Level	Reliability	R_{system}	R_{load}
AC	grid to PDU	0.97920788125372	0.97664527114055	0.97747320385153
	PDU to rack	0.99999457918603		
	Rectifier	0.97790126122819		
DC	grid to PDU	0.96839571120014	0.99697298323125	0.99890732896361
	PDU to rack	0.99990606621017		

Although the DC grid-to-PDU segment shows slightly lower individual reliability than its AC counterpart due to utilizing different components and adding the rectifier upstream, the overall DC system reliability is higher. This is due to the reduced number of elements in series, which limits the failure probabilities across the system. In the AC architecture, the presence of additional power electronic stages (particularly the inverter) introduces extra failure points that reduce long-term reliability.

5.7.3. Availability vs. Reliability Interpretation

The results clearly demonstrate that availability and reliability capture different physical aspects of system performance:

- Availability is dominated by repairability (MTTR) and benefits strongly from redundancy.
- Reliability is governed by failure occurrence (MTBF) over time and is more sensitive to the number of components connected in series.

Consequently, it is possible—and observed in this study—that both architectures achieve extremely high availability values, while their reliability differs more noticeably over the mission time. DC architecture combines higher availability and higher reliability, primarily due to architectural simplification and reduced dependence on power electronic conversion stages.

The key observations can be summarized as follows:

- ✓ DC architecture exhibits superior availability at both system and load levels.
- ✓ DC architecture also demonstrates higher reliability over the considered mission time, despite identical assumptions.
- ✓ The elimination of the rack-level rectifier and the reduction in serial components are the dominant factors driving the improvement.
- ✓ The numerical results should be interpreted as relative performance metrics, suitable for comparing architectures rather than predicting absolute operational behavior.

5.7.4. Future Improvements

Given the significantly higher availability and reliability achieved by the proposed DC architecture, the resulting performance margins may exceed typical data center requirements. This creates the opportunity to reduce redundancy levels while still meeting target availability and reliability criteria.

For instance, the upstream section, currently modeled with a 3-to-make-2 (2oo3) redundancy, could be redesigned using an N+1 redundancy scheme. Such a configuration would reduce the number of parallel units by one (e.g., one fewer UPS, UDP, and other associated equipment), while maintaining acceptable system performance.

In addition, the DC nature of the distribution system enables alternative network topologies, such as ring or meshed configurations as shown in Figure 11. Unlike AC distribution, DC architecture is not affected by classical harmonic circulation or reactive power interactions between parallel feeders. While power electronic converters can introduce current ripples and high frequency noise, these effects are fundamentally different from AC harmonics and are typically addressed through filtering and proper converter design. A ring configuration can improve supply continuity by allowing power to reach the load from multiple directions, potentially reducing the need for fully duplicated equipment.

Together, reduced redundancy levels and the adoption of ring-based DC distribution could lead to further reductions in installed equipment, footprint, losses, Operational Expenditure (Op-Ex), and mostly Capital Expenditure (Cap-Ex). These savings may partially or fully offset the higher unit cost of DC rated components, such as DC circuit breakers. It should be emphasized that these considerations represent design opportunities enabled by the improved reliability and structural simplicity of DC systems, and would require detailed, project-specific validation before implementation.

6 Summary and Scope

6.1. Overall Comparison

The availability and reliability analysis demonstrates that the proposed DC distribution architecture consistently outperforms the AC reference system at both system and load levels under identical modeling assumptions. While both architectures achieve very high steady-state availability due to extensive redundancy, the DC configuration benefits from a reduced number of series components and power-conversion stages, resulting in significantly lower unavailability and a higher probability of uninterrupted operation over the considered mission time. It is emphasized that the numerical values obtained using standardized IEEE reliability data should be interpreted as comparative indicators rather than absolute predictions of field performance.

The resulting performance margins indicate that DC architecture not only improves availability and reliability but also enables new design opportunities. Redundancy levels may be reduced (such as adopting an N+1 scheme instead of a 3-to-make-2 configuration) while still meeting target service-continuity requirements. Furthermore, the intrinsic characteristics of DC distribution allow alternative network topologies, including ring or meshed configurations, which are difficult to implement in AC systems due to synchronization, reactive power flow, and harmonic constraints. These opportunities could lead to further reductions in installed equipment, footprint, and expenditure. Although a detailed evaluation of such architectures is beyond the scope of this work, the results confirm that DC distribution provides not only higher performance but also greater flexibility for future optimization of data-center power systems.

An overall comparison of all the aspects considered in this study is demonstrated in Table 14.

Table 14. An Overall Comparison

Metric	AC	DC (min CSA)	DC (constant J)
Total cable mass [t]	536.23	298.06	418.7
Cable cost [M€]	7.26	4.81	5.39
Annual energy loss [MWh]	3278	1102	693
Avg. power loss [kW]	373.2	125.4	78.93
Power loss cost [k€]	593	199.5	125.4
System availability	0.999992	0.999999	-
System reliability (5 years)	0.9766	0.9970	-

Table 14 provides a high-level comparison between the AC and DC power-distribution architectures across key technical metrics. The results indicate that DC solutions achieved a significant reduction in copper usage and associated cable costs, together with lower electrical losses and higher availability, compared to the conventional AC architecture. Differences between the two DC cases reflect alternative conductor-sizing criteria, while system-level reliability depends on the architectural configuration rather than by conductor selection.

In addition, Figure 26 presents a normalized graphical representation of the results summarized in Table 14. In this figure, the AC configuration is taken as the reference case and set to 100%, while the corresponding DC values are expressed as a percentage of the AC system. This approach allows a direct visual comparison of relative performance across multiple metrics with different physical units.

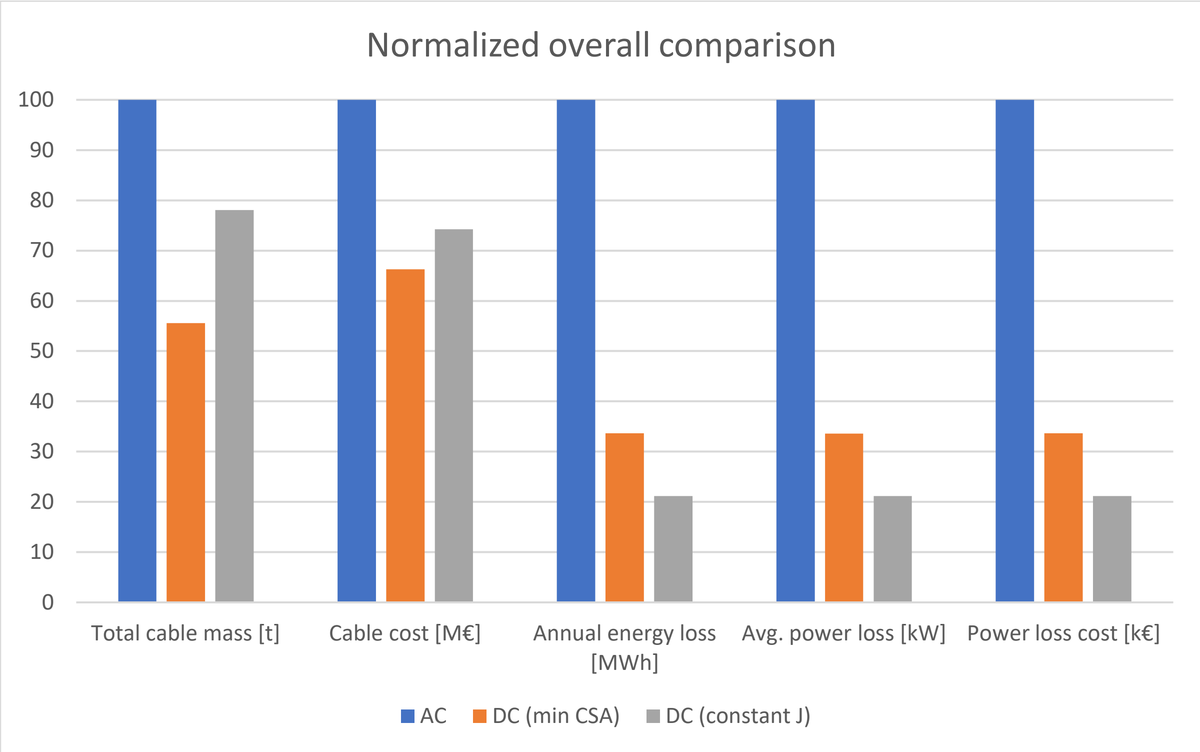

Figure 26. material, efficiency, and cost comparison

The chart clearly illustrates that both DC configurations significantly reduce annual energy losses, average power losses, and loss-related operational costs. In particular, the DC (constant current density) case exhibits the lowest loss values, reflecting the impact of larger conductor cross-sections on resistive losses. The DC (minimum CSA) case, on the other hand, achieves the lowest total cable mass and material cost, demonstrating the effect of conductor downsizing.

The difference between copper volume reduction and total cable mass reduction can also be observed graphically. While copper usage decreases substantially, the total cable mass reduction is slightly lower due to the presence of insulation and sheath materials, which remain proportional to the selected conductor size and partially limit the overall mass reduction.

Overall, the normalized comparison highlights the structural advantages of the DC architecture in terms of material efficiency and operational performance, while clearly distinguishing the effects of the two conductor-sizing strategies.

For the availability and reliability comparison, Figure 27 compares the system-level availability and five-year reliability of the AC and DC architectures. The results show that both systems achieve very high availability levels, consistent with data center design requirements. However, the DC architecture demonstrates a measurable improvement.

The improvement in reliability is more pronounced than in availability. Over a five-year horizon, the DC configuration achieves a higher reliability value due to the reduced number of conversion stages, and the elimination of certain intermediate components present in the AC topology. This structural simplification decreases the overall failure probability of the system.

It is important to note that availability values are very close to unity in both cases, and therefore small numerical differences correspond to meaningful reductions in expected downtime (from hundreds of seconds to milliseconds). The graphical representation makes this difference more visible and supports the quantitative results reported in Table 14.

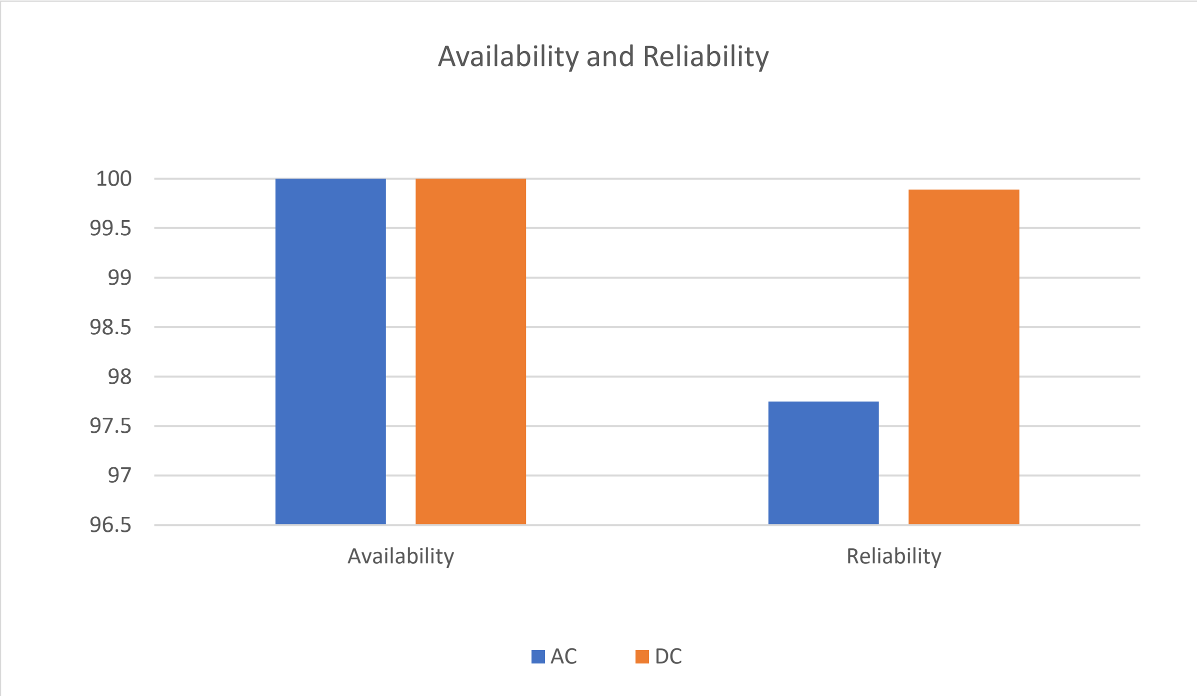

Figure 27. Availability and reliability comparison

6.2. Scope and limitations

This work presents a comparative analysis of AC and DC power distribution architectures for hyperscale data centers, focusing on conductor sizing, copper usage, electrical losses, availability, and reliability under a consistent set of assumptions. Since the objective of this thesis is not a detailed analysis of a specific subsystem, but a more general analysis for the whole system, there are some aspects that are not considered/neglected in this work that can be considered for future work or for a more specified study.

To ensure clarity and correct interpretation of the results, the main scope limitations are summarized below.

6.2.1. System Topology Scope

The study assumes identical routing, load distribution, and redundancy criteria for both AC and DC architectures to ensure a fair comparison. Dynamic load growth, adaptive reconfiguration, and advanced meshed or ring-based DC topologies are not quantitatively evaluated, although the reliability results indicate that such configurations represent promising opportunities for future optimization.

In addition, the adopted comparison maintains functionally equivalent power paths in the AC and DC models. In practice, DC architecture may allow further topological simplifications, such as potentially eliminating the need for bypasses for the UPS path in the AC system. Such simplifications could modify system reliability characteristics and further reduce Cap-Ex; however, these effects are not included in the present analysis to preserve model consistency.

6.2.2. Economic Modeling Assumptions

The cost analysis focuses exclusively on cable material costs and copper usage. Installation labor, containment systems, protection devices, transportation, taxes, and lifecycle operational costs are excluded.

Further limitation concerns the cost of electrical equipment. DC architectures may involve higher unit costs for certain components, such as DC circuit breakers and protection devices, which are not explicitly considered in the present analysis. However, these higher component costs may be partially or fully offset by simplifications enabled by DC distribution, including reduced power conversion stages, simplified power paths, and reduced cable costs, as discussed throughout this study.

It should also be noted that low-voltage DC distribution in large-scale data centers is not yet supported by the same level of standardization, product maturity, and market penetration as conventional AC systems. The limited availability of standardized DC-rated components and protection solutions may introduce additional engineering complexity, vendor dependency, and cost uncertainty, particularly in early-stage implementations.

However, ongoing technological advancements and increasing adoption of DC equipment are contributing to a gradual reduction in component costs, while the technology is also moving toward improved standardization and broader industrial acceptance. As a result, the current limitations related to component availability and interoperability are expected to diminish. Consequently, it is plausible that, at system level, future DC implementations may achieve comparable or even lower Cap-Ex than conventional AC solutions.

6.2.3. Electrical Modeling Assumptions

The electrical analysis is based on steady state operation at fundamental frequency. Harmonic currents generated by nonlinear loads are not explicitly modeled. In practice, such harmonics increase conductor and transformer losses in AC systems, while DC distribution inherently avoids low frequency harmonic propagation. As a result, the loss reduction associated with DC architecture may be conservatively estimated in this study.

Transient phenomena, including inrush currents, short circuit behavior, and fault clearing dynamics, are outside the scope of the analysis. Voltage drops and losses are evaluated under rated operating conditions and worst-case steady state loading scenarios.

6.2.4. Protection and Control Aspects

Protection coordination, selectivity, and fault isolation strategies are not explicitly modeled. In particular, the dynamic behavior of DC circuit breakers, fault detection delays, and coordination between protection devices are not considered. While these aspects are critical for practical DC system implementation, their detailed analysis requires time domain simulations and manufacturer specific data which is beyond the scope of this work.

6.2.5. Reliability and Modeling

Availability and reliability are evaluated using Reliability Block Diagrams (RBDs) and generic component data derived from IEEE Std. 493. The analysis assumes statistically independent component failures and constant failure and repair rates. Common cause failures, shared environmental dependencies, and maintenance outages are not explicitly captured and may reduce real world performance compared to idealized RBD results.

It should be noted that some IEEE 493 entries report zero restoration time; these values are retained as given to preserve source consistency and because the objective is a comparative assessment.

Components upstream of the MV/LV transformer are modeled as highly reliable to isolate the impact of internal distribution architectures. This assumption increases absolute availability values and reinforces the interpretation of the results as comparative indicators rather than exact field predictions.

6.2.6. Thermal and Cooling System Considerations

The electrical loss reduction calculated for the DC distribution architecture may also lead to indirect benefits at the thermal management level. Lower distribution losses and elimination of power electronic equipment result in reduced heat dissipation within electrical rooms, cable trays, and rack level infrastructure. Therefore, the cooling system may operate with lower thermal loads, potentially reducing cooling energy consumption and, in some cases, allowing for a lower number or smaller rating of cooling units.

However, the interaction between electrical losses and cooling system performance is not explicitly modeled in this study. Detailed thermal simulations, airflow modeling, and cooling system control strategies are outside the scope of the present work. As a result, the overall energy efficiency benefits of DC architecture may be conservatively estimated in this analysis.

Despite these limitations, the adopted modeling framework provides a consistent and transparent basis for comparing AC and DC distribution architectures and highlights the key mechanisms driving differences in efficiency, material usage, and reliability.

7 Conclusion

This thesis investigated the potential advantages of adopting bipolar 800 V DC (± 400 V DC) power distribution architecture in a large-scale data center, compared to a conventional low voltage AC solution. The analysis focused on three key technical dimensions that directly influence data center design and operation: copper usage and conductor sizing, electrical losses during operation, and system availability and reliability.

The conductor sizing analysis demonstrated that the higher distribution voltage of DC architecture leads to a significant reduction in current levels for the same delivered power. Therefore, smaller conductor cross sections can be adopted across multiple distribution levels, resulting in a substantial reduction in total copper usage. Since cable costs are strongly correlated with cable mass, this reduction translates into a large potential decrease in Cap-Ex.

The electrical loss analysis, based on measured operational data over one year, showed that DC architecture achieves lower distribution losses compared to the AC system. The elimination of inverter stages and the reduction of current related losses contribute to improved overall efficiency. While the absolute magnitude of energy savings depends on load profiles and operational conditions, the results confirm that DC distribution can provide measurable reductions in annual energy losses, with associated economic (Op-Ex) and environmental benefits.

From a reliability and availability perspective, the DC architecture exhibited superior performance at both system and load levels. The reduced number of conversion stages and the simplified power path result in fewer critical components contributing to failure. The availability analysis indicates that, under the adopted assumptions, the proposed DC solution can exceed typical data center availability requirements. This opens the possibility of reevaluating redundancy strategies, such as reducing the number of parallel components or adopting alternative topologies, while maintaining high availability targets and further reducing capital costs.

Overall, the results of this work confirm that bipolar 800 V DC distribution represents a technically viable and advantageous alternative to conventional AC architectures for large-scale data centers. While AC systems remain mature and widely standardized, the demonstrated reductions in copper usage, electrical losses, and component induced unavailability highlight the potential of DC solutions in future high efficiency and high reliability facilities.

Further works may extend the present analysis to include harmonic effects, protection coordination, dynamic load growth, and detailed lifecycle cost assessments, to fully quantify the long-term benefits of DC distribution.

In addition, future investigations may focus on the integration of advanced cooling technologies and waste heat recovery solutions to further improve the overall energy efficiency of data centers. Other extensions may include the evaluation of electromagnetic interference mitigation through filtering solutions, more detailed component level failure modeling, and the integration of alternative energy storage technologies such as supercapacitors or flywheels. Finally, the optimization of UPS operating strategies, like economic mode optimization, could be analyzed to further enhance system efficiency, availability, and reliability under real operating conditions.

Bibliography

[1] K. Jiang *et al.*, “Energy Efficiency Evaluation and Revenue Distribution of DC Power Distribution Systems in Nearly Zero Energy Buildings,” *Energies (Basel).*, vol. 15, no. 15, Aug. 2022, doi: 10.3390/en15155726.

[2] A. Beloglazov, R. Buyya, Y. C. Lee, and A. Zomaya, “A Taxonomy and Survey of Energy-Efficient Data Centers and Cloud Computing Systems.”

[3] S. Bharany *et al.*, “A Systematic Survey on Energy-Efficient Techniques in Sustainable Cloud Computing,” *Sustainability (Switzerland)*, vol. 14, no. 10, May 2022, doi: 10.3390/su14106256.

[4] A. Shehabi *et al.*, “United States Data Center Energy Usage Report,” 2016.

[5] K. Bilal *et al.*, “A taxonomy and survey on Green Data Center Networks,” *Future Generation Computer Systems*, vol. 36, pp. 189–208, 2014, doi: 10.1016/j.future.2013.07.006.

[6] D. Mytton and M. Ashtine, “Sources of data center energy estimates: A comprehensive review,” Sep. 21, 2022, *Cell Press*. doi: 10.1016/j.joule.2022.07.011.

[7] H. Fuchs *et al.*, “Recalibrating global data center energy-use estimates,” *Energy Effic.*, vol. 13, no. 3, pp. 379–392, Mar. 2020, doi: 10.1007/s12053-019-09809-8.

[8] E. Masanet, N. Lei, and J. Koomey, “To better understand AI’s growing energy use, analysts need a data revolution,” Sep. 18, 2024, *Cell Press*. doi: 10.1016/j.joule.2024.07.018.

[9] G. Kamiya and V. C. Coroamă, “Data Centre Energy Use: Critical Review of Models and Results,” 2025. [Online]. Available: www.iea-4e.org/edna

[10] M. J. Almheiri, H. M. Khalid, A. Ismail, A. Gulraiz, and Z. Said, “Chilled water-based hybrid cooling solution for data centers: a comprehensive survey of technologies, developments, and regenerative energy transitions,” *Energy Conversion and Management: X*, p. 101612, Jan. 2026, doi: 10.1016/j.ecmx.2026.101612.

[11] M. Stahlhut, M. Sekulla, P. Großöhme, A. Auweter, and T. Urbaneck, “Data Centers With Direct Liquid-Cooled Servers: Experimental Analysis and Modeling,” *Energy Sci. Eng.*, vol. 13, no. 7, pp. 3605–3619, Jul. 2025, doi: 10.1002/ese3.70116.

[12] L. Simon, S. Research Associate, U. Institute, D. Bizo, and R. Director, “Vendor view: Uptime Institute Direct Liquid Cooling Survey 2022,” 2022. [Online]. Available: www.uptimeinstitute.com

[13] X. Yuan, Y. Liang, X. Hu, Y. Xu, Y. Chen, and R. Kosonen, "Waste heat recoveries in data centers: A review," Dec. 01, 2023, *Elsevier Ltd*. doi: 10.1016/j.rser.2023.113777.

[14] M. Noro, L. Zhang, Z. Zhao, B. Chen, M. Zhao, and Y. Chen, "Zero-Carbon Development in Data Centers Using Waste Heat Recovery Technology: A Systematic Review," 2025, doi: 10.3390/s10.3390/su172210101.

[15] Y. Zhang, S. Member, D. C. Wilson, I. Ch Paschalidis, A. K. Coskun, and S. Member, "HPC Data Center Participation in Demand Response: an Adaptive Policy with QoS Assurance," 2020.

[16] Y. Wang *et al.*, "Data center integrated energy system for sustainability: Generalization, approaches, methods, techniques, and future perspectives," Feb. 26, 2024, *Innovation Press*. doi: 10.59717/j.xinn-energy.2024.100014.

[17] P. Ziaei, O. Husev, and J. Rabkowski, "Data Centers as a Driving Force for the Renewable Energy Sector," Jan. 01, 2026, *Multidisciplinary Digital Publishing Institute (MDPI)*. doi: 10.3390/en19010236.

[18] J. Irion, P. Wiesner, J. Bader, and O. Kao, "Optimizing Microgrid Composition for Sustainable Data Centers," Sep. 2025, [Online]. Available: http://arxiv.org/abs/2508.04284

[19] I. Riepin, T. Brown, and V. M. Zavala, "Spatio-temporal load shifting for truly clean computing," *Advances in Applied Energy*, vol. 17, Mar. 2025, doi: 10.1016/j.adapen.2024.100202.

[20] E. Rodrigues, J. Goldverg, and T. Kosar, "Carbon-Aware Temporal Data Transfer Scheduling Across Cloud Datacenters," Jun. 2025, [Online]. Available: http://arxiv.org/abs/2506.04117

[21] H. E. Gelani, F. Dastgeer, M. Nasir, S. Khan, and J. M. Guerrero, "Ac vs. Dc distribution efficiency: Are we on the right path?," Jul. 01, 2021, *MDPI AG*. doi: 10.3390/en14134039.

[22] D. L. Gerber, V. Vossos, W. Feng, C. Marnay, B. Nordman, and R. Brown, "A simulation-based efficiency comparison of AC and DC power distribution networks in commercial buildings," *Appl. Energy*, vol. 210, pp. 1167–1187, Jan. 2018, doi: 10.1016/j.apenergy.2017.05.179.

[23] V. Vossos, D. Gerber, Y. Bennani, R. Brown, and C. Marnay, "Techno-economic analysis of DC power distribution in commercial buildings," *Appl. Energy*, vol. 230, pp. 663–678, Nov. 2018, doi: 10.1016/j.apenergy.2018.08.069.

[24] S. Li, T. Zhang, and X. Liu, "Techno-economic performance of different DC power distribution networks in official buildings based on a real-time analysis method," *Energy Build.*, vol. 325, Dec. 2024, doi: 10.1016/j.enbuild.2024.114996.

[25] D. Sreenivasarao, P. Agarwal, and B. Das, "Neutral current compensation in three-phase, four-wire systems: A review," May 2012. doi: 10.1016/j.epsr.2011.12.014.

[26] M. Glinkowski *et al.*, "DATA CENTER POWER SYSTEM HARMONICS: AN OVERVIEW OF EFFECTS ON DATA CENTER EFFICIENCY AND RELIABILITY."

[27] G. N. C. Ferguson, "POWER QUALITY IMPROVEMENT IN A HARMONIC ENVIRONMENT," 1997.

[28] T. D. Kefalas and A. G. Kladas, "Harmonic impact on distribution transformer no-load loss," *IEEE Transactions on Industrial Electronics*, vol. 57, no. 1, pp. 193–200, Jan. 2010, doi: 10.1109/TIE.2009.2030207.

[29] M. Yazdani-Asrami, M. Mirzaie, and A. A. Shayegani Akmal, "No-load loss calculation of distribution transformers supplied by nonsinusoidal voltage using three-dimensional finite element analysis," *Energy*, vol. 50, no. 1, pp. 205–219, Feb. 2013, doi: 10.1016/j.energy.2012.09.050.

[30] L. Giuntini, A. Mannuccini, L. Giuntini, and A. Mannuccini, "Double-conversion UPS efficiency under varying mains conditions," 2013.

[31] L. Giuntini, "Harmonics Reduction in High-Efficiency Operation of Double-Conversion UPS," 2011.

[32] "Efficiency beyond the AC based datacenter designs; 400VDC power feed solution," 2018.

[33] B. R. Shrestha, "Efficiency and Reliability Analysis of AC and 380V DC Data Efficiency and Reliability Analysis of AC and 380V DC Data Centers Centers." [Online]. Available: https://openprairie.sdstate.edu/etd

[34] V. A. Prabhala, B. P. Baddipadiga, P. Fajri, and M. Ferdowsi, "An overview of direct current distribution system architectures & benefits," Sep. 01, 2018, *MDPI AG*. doi: 10.3390/en11092463.

[35] "380 Vdc Architectures for the Modern Data Center." [Online]. Available: www.EMergeAlliance.org

[36] M. T. Pueschel, "DC-Powered Office Buildings and Data Centres The First 380 VDC Micro Grid in a Commercial Building in Germany."

[37] R. B. Darla and A. Chitra, "A comprehensive review of distributed power system architecture for telecom and datacenter applications," *International Journal of Power Electronics and Drive Systems*, vol. 12, no. 3, pp. 1535–1555, Sep. 2021, doi: 10.11591/ijpeds.v12.i3.pp1535-1555.

[38] F. Bodi, *380/400V DC Powering Option An Independent Review*. IEEE, 2011.

[39] F. Ghazanfar, “Modeling of LVDC Distribution System: An Assessment of Control, Power Quality, and DC Faults,” 2018.

[40] B. Wunder *et al.*, “Energy Efficient DC-Grids for Commercial Buildings.”

[41] *Power System Architectures for 380V DC Distribution in Telecom Datacenters*. IEEE, 2012.

[42] “PRESS RELEASE: Electricity: from 1 July 3.7 million non-vulnerable customers on the Standard Offer Service automatically switch to the Gradual Standard Offer Service.” [Online]. Available: https://www.arera.it/dati-e-statistiche/dettaglio/analisi-dei-consumi-

[43] G. . Pasaoglu, C. . Thiel, A. . Martino, A. . Zubaryeva, D. . Fiorello, and L. . Zani, *Projections for electric vehicle load profiles in Europe based on travel survey data*. Publications Office, 2013.

[44] “Greenhouse gas emission intensity of electricity generation, country level | Greenhouse gas emission intensity of electricity generation in Europe | European Environment Agency (EEA).” Accessed: Feb. 04, 2026. [Online]. Available: https://www.eea.europa.eu/en/analysis/indicators/greenhouse-gas-emission-intensity-of-1-1751032678/greenhouse-gas-emission-intensity-of-electricity-generation-country-level

[45] “How much CO2 does a tree absorb? | Viessmann UK.” Accessed: Feb. 04, 2026. [Online]. Available: https://www.viessmann.co.uk/en/heating-advice/boilers/how-much-co2-does-tree-absorb.html?

A Appendix A

This appendix provides a representative Python script used in the data processing workflow for the loss calculations presented in Chapter 4. The complete workflow consisted of multiple scripts for data extraction, cleaning, aggregation, and loss computation; however, only the script related to square-currents calculations is reported here as an illustrative example.

The script performs a preprocessing step on measured operational datasets exported in Excel format. Specifically, it reads one or more .xlsx files containing a timestamp column followed by one or more measurement columns (e.g., phase currents). Since some exported datasets use the decimal comma convention, numeric values are converted to floating-point format before further processing. The script then computes the squared value of each measurement sample, which is required for subsequent Joule-loss calculations based on I^2R. The processed output is saved as a new Excel file in the same directory as the input file, using the “filename” _square.xlsx name.

Input assumptions are as follows: (I) the first column contains the timestamp or sample index and is preserved unchanged; (II) all remaining columns contain numeric measurements; and (III) empty or non-numeric cells are coerced to zero to allow batch processing without interruption.

```
import os
import pandas as pd
from tkinter import Tk, filedialog

def read_excel_with_decimal_comma(path: str) -> pd.DataFrame:
    """
    Read an Excel file and convert decimal-comma numbers to floats.
    """
    df = pd.read_excel(path, engine="openpyxl")
    return df

def drop_columns_without_header(df: pd.DataFrame) -> pd.DataFrame:
    """
    Remove columns that do not have a real header.
```

```
    """
    good_cols = []
    for col in df.columns:
        if pd.isna(col):
            continue
        if isinstance(col, str) and col.strip() == "":
            continue
        good_cols.append(col)
    return df.loc[:, good_cols]

def to_numeric_decimal_comma(series: pd.Series) -> pd.Series:
    """
    Convert a column that may contain decimal-comma strings to numeric.
    Empty cells become 0.
    """
    # If already numeric, keep it
    if pd.api.types.is_numeric_dtype(series):
        return series.fillna(0)

    # Convert everything to string, replace comma with dot, then coerce to numeric
    s = series.astype(str).str.replace(",", ".", regex=False)
    s = pd.to_numeric(s, errors="coerce").fillna(0)
    return s

def main():
    # Hide the root Tk window
    root = Tk()
    root.withdraw()

    # Ask how many files to process
    n_files = int(input("How many .xlsx files do you want to analyze? ").strip())

    for i in range(1, n_files + 1):
        print(f"\nSelect file {i} of {n_files}...")
        in_path = filedialog.askopenfilename(
            title=f"Select input Excel file ({i}/{n_files})",
            filetypes=[("Excel files", "*.xlsx")],
        )

        if not in_path:
            print("No file selected. Skipping this entry.")
            continue
```

```
        try:
            # Read
            df = read_excel_with_decimal_comma(in_path)

            # Remove columns without header
            df = drop_columns_without_header(df)

            if df.shape[1] < 2:
                raise ValueError("File must have at least 2 columns (timestamp +
data).")

            # Keep timestamp (first column) as-is
            ts_col_name = df.columns[0]
            out_df = pd.DataFrame()
            out_df[ts_col_name] = df.iloc[:, 0]

            # Convert all data columns to numeric (decimal comma) and square them
            data_cols = df.columns[1:]
            for col in data_cols:
                numeric_col = to_numeric_decimal_comma(df[col])
                out_df[col] = numeric_col.pow(2)

            # Save to same folder as input
            folder = os.path.dirname(in_path)
            stem = os.path.splitext(os.path.basename(in_path))[0]
            out_path = os.path.join(folder, f"{stem}_square.xlsx")

            out_df.to_excel(out_path, index=False, engine="openpyxl")
            print(f"Saved: {out_path}")

        except Exception as e:
            print(f"ERROR processing file: {in_path}\n{e}")

if __name__ == "__main__":
    main()
```

B Appendix B

This appendix presents the Python implementation used to compute the availability and reliability of the AC and DC distribution architectures described in Chapter 5.

The model is based on a nested Reliability Block Diagram (RBD) representation, where system topology is defined through external JSON files and component reliability parameters are provided via CSV input files.

The implementation computes:

- Steady state availability using MTBF and MTTR values
- System reliability over a 5-year mission time
- System unavailability
- Probability of failure within the mission period

The following assumptions are adopted:

- Independent component failures
- Constant failure rate (exponential distribution)

Reliability parameters are derived from IEEE Std. 493 (Gold Book).

B.1 Python Reliability Script

The reliability and availability calculations presented in Chapter 5 were implemented in Python. The script loads:

- A topology definition file in JSON format
- A component reliability database in CSV format

The model evaluates RBD using a recursive approach.

The following functions are implemented:

- Steady-state availability

$$A = \frac{MTBF}{MTBF + MTTR}$$

- Exponential reliability over a mission time t

$$R(t) = e^{-\frac{t}{MTBF}}$$

- Series configuration: product of block values
- Parallel configuration:

$$1 - \prod(1 - X_i)$$

The mission time used for reliability evaluation is 5 years (43,800 hours).

```
import json
import csv
import math
from typing import Any, Dict, List, Tuple, Union
import networkx as nx
import matplotlib.pyplot as plt
# =========================
# USER SETTINGS (PATHS)
# =========================
TOPOLOGY_PATH = "topology.json"
COMPONENTS_PATH = "components.csv"

# Formatting preference
def fmt15(x: float) -> str:
    return f"{x:.15f}"

# =========================
# USER SETTINGS (MISSION TIME)
# =========================

MISSION_TIME_YEARS = 5
MISSION_TIME_HR = MISSION_TIME_YEARS * 365 * 24

# =========================
# AVAILABILITY MODELS
# =========================

def availability_from_mtbf_mttr(mtbf_hr: float, mttr_hr: float) -> float:
    """
        A = MTBF / (MTBF + MTTR)
    """
    if mtbf_hr <= 0:
        raise ValueError(f"MTBF must be > 0, got {mtbf_hr}")
    if mttr_hr < 0:
        raise ValueError(f"MTTR must be >= 0, got {mttr_hr}")
```

```
    return mtbf_hr / (mtbf_hr + mttr_hr)

def parallel_availability(A_list: List[float]) -> float:
    """
        A = 1 - Π(1 - Ai)
    """
    prod_down = 1.0
    for Ai in A_list:
        prod_down *= (1 - Ai)
    return 1.0 - prod_down

# ========================
# RELIABILITY MODELS (EXPONENTIAL)
# ========================

def reliability_from_mtbf_exponential(mtbf_hr: float, t_hr: float) -> float:
    """
        R(t) = exp(-t/MTBF)
    """
    if mtbf_hr <= 0:
        raise ValueError(f"MTBF must be > 0, got {mtbf_hr}")
    if t_hr < 0:
        raise ValueError(f"Mission time t must be >= 0, got {t_hr}")
    return math.exp(-t_hr / mtbf_hr)

def parallel_reliability(R_list: List[float]) -> float:
    """
        R = 1 - Π(1 - Ri)
    """
    prod_fail = 1.0
    for Ri in R_list:
        prod_fail *= (1.0 - Ri)
    return 1.0 - prod_fail

# ========================
# LOADING FILES (ROBUST)
# ========================

def load_topology(path: str) -> Dict[str, Any]:
    """
    topology.json. Must contain:
       root
```

```
    """
    with open(path, "r", encoding="utf-8-sig") as f:
        return json.load(f)


def load_components(path: str) -> Dict[str, Dict[str, float]]:
    """
    Supports:
      - UTF-8 BOM (utf-8-sig)
      - delimiter ',' or ';' (auto-detect)
      - headers with extra spaces
      - skips empty rows

    Required columns:
      component name, mtbf_hr, mttr_hr

    Returns:
      comp_data[name] = {"mtbf_hr":xxx, "mttr_hr":xxx, "A":xxx}
    """
    comp_data: Dict[str, Dict[str, float]] = {}

    with open(path, "r", encoding="utf-8-sig", newline="") as f:
        first_line = f.readline()
        delimiter = ";" if ";" in first_line else ","
        f.seek(0)

        reader = csv.DictReader(f, delimiter=delimiter)

        if reader.fieldnames is None:
            raise ValueError("CSV appears to have no header row.")

        # Normalize header names
        reader.fieldnames = [h.strip().lower() for h in reader.fieldnames]

        required = {"component", "mtbf_hr", "mttr_hr"}
        missing = required - set(reader.fieldnames)
        if missing:
            raise ValueError(
                f"CSV missing required columns: {missing}. "
                f"Found columns: {reader.fieldnames}"
            )

        for row in reader:
```

```
            # Skip empty rows
            if  not  row  or  all((v  is  None  or  str(v).strip()  ==  "")  for  v  in
row.values()):
                continue

            # Normalize keys/values
            row = {k.strip().lower(): (v.strip() if isinstance(v, str) else v) for k,
v in row.items()}

            name = row["component"].strip()
            if not name:
                continue

            try:
                mtbf = float(row["mtbf_hr"])
                mttr = float(row["mttr_hr"])
            except Exception as e:
                raise ValueError(f"Invalid MTBF/MTTR for component '{name}': {row}")
from e

            A = availability_from_mtbf_mttr(mtbf, mttr)
            comp_data[name] = {"mtbf_hr": mtbf, "mttr_hr": mttr, "A": A}

    return comp_data

def is_bundle(node) -> bool:
    return isinstance(node, dict) and node.get("_type") == "bundle"

def make_bundle(names: list) -> dict:
    return {"_type": "bundle", "names": names}

def compress_consecutive_strings(nodes: list, no_bundle: set) -> list:
    out = []
    buf = []

    def flush():
        nonlocal buf
        if buf:
            out.append(make_bundle(buf) if len(buf) > 1 else buf[0])
            buf = []

    for n in nodes:
        if isinstance(n, str):
```

```
            if n in no_bundle:
                flush()
                out.append(n)
            else:
                buf.append(n)
        else:
            flush()
            out.append(n)

    flush()
    return out

# ========================
# RECURSIVE EVALUATION
# ========================
Node = Union[str, Dict[str, Any]]


def get_component_A(comp_name: str, comp_data: Dict[str, Dict[str, float]]) -> float:
    if not isinstance(comp_name, str):
        raise TypeError(f"Component name must be a string, got {type(comp_name)}: {repr(comp_name)}")
    comp_name = comp_name.strip()
    if comp_name not in comp_data:
        sample = list(comp_data.keys())[:15]
        raise KeyError(
            f"Component '{comp_name}' not found in components.csv. "
            f"Sample available names: {sample}"
        )
    return comp_data[comp_name]["A"]


def get_component_R(comp_name: str, comp_data: Dict[str, Dict[str, float]], t_hr: float) -> float:
    if not isinstance(comp_name, str):
        raise TypeError(f"Component name must be a string, got {type(comp_name)}: {repr(comp_name)}")
    comp_name = comp_name.strip()
    if comp_name not in comp_data:
        sample = list(comp_data.keys())[:15]
        raise KeyError(
            f"Component '{comp_name}' not found in components.csv. "
            f"Sample available names: {sample}"
        )
```

```
    mtbf = comp_data[comp_name]["mtbf_hr"]
    return reliability_from_mtbf_exponential(mtbf, t_hr)

def eval_node(node: Node, comp_data: dict) -> float:
    if isinstance(node, str):
        return get_component_A(node, comp_data)

    if is_bundle(node):
        A = 1.0
        for name in node["names"]:
            A *= get_component_A(name, comp_data)
        return A

    if isinstance(node, dict):
        return compute_block_availability(node, comp_data)

    raise TypeError(f"Invalid node type: {type(node)} with value {repr(node)}")

def compute_block_availability(block: Dict[str, Any], comp_data: Dict[str, Dict[str,
float]]) -> float:

    """
    Supported blocks:
      - series:
          {"type":"series","items":[node,node,...]}

      - parallel:
          {"type":"parallel","branches":[ [node,...], [node,...], ... ]}
    """

    if "type" not in block:
        raise KeyError(f"Block missing 'type': {block}")

    btype = block["type"]

    if btype == "series":
        items = block.get("items", None)
        if items is None:
            items = block.get("components", [])
        if not isinstance(items, list):
            raise TypeError(f"series.items must be a list, got {type(items)}")

        A = 1.0
```

```
        for it in items:
            A *= eval_node(it, comp_data)
        return A

    if btype == "parallel":
        branches = block.get("branches", None)
        if branches is None:
            comps = block.get("components", [])
            branches = [[c] for c in comps]

        if not isinstance(branches, list) or any(not isinstance(b, list) for b in
branches):
            raise TypeError("parallel.branches must be a list of lists")

        A_branches: List[float] = []
        for branch in branches:
            A_b = 1.0
            for it in branch:
                A_b *= eval_node(it, comp_data)
            A_branches.append(A_b)

        return parallel_availability(A_branches)


    raise ValueError(f"Unsupported block type: {btype}")


def eval_node_reliability(node: Node, comp_data: dict, t_hr: float) -> float:
    if isinstance(node, str):
        return get_component_R(node, comp_data, t_hr)

    if is_bundle(node):
        R = 1.0
        for name in node["names"]:
            R *= get_component_R(name, comp_data, t_hr)
        return R

    if isinstance(node, dict):
        return compute_block_reliability(node, comp_data, t_hr)

    raise TypeError(f"Invalid node type: {type(node)} with value {repr(node)}")
```

```
def compute_block_reliability(block: Dict[str, Any], comp_data: Dict[str, Dict[str,
float]], t_hr: float) -> float:

    """
      - series: multiply
      - parallel: 1 - Π(1 - Ri)
    """

    if "type" not in block:
        raise KeyError(f"Block missing 'type': {block}")

    btype = block["type"]

    if btype == "series":
        items = block.get("items", None)
        if items is None:
            items = block.get("components", [])
        if not isinstance(items, list):
            raise TypeError(f"series.items must be a list, got {type(items)}")

        R = 1.0
        for it in items:
            R *= eval_node_reliability(it, comp_data, t_hr)
        return R

    if btype == "parallel":
        branches = block.get("branches", None)
        if branches is None:
            comps = block.get("components", [])
            branches = [[c] for c in comps]

        if not isinstance(branches, list) or any(not isinstance(b, list) for b in
branches):
            raise TypeError("parallel.branches must be a list of lists")

        R_branches: List[float] = []
        for branch in branches:
            R_b = 1.0
            for it in branch:
                R_b *= eval_node_reliability(it, comp_data, t_hr)
            R_branches.append(R_b)

        return parallel_reliability(R_branches)
```

```
    raise ValueError(f"Unsupported block type: {btype}")


# =========================
# DRAWING
# =========================

BRANCH_Y_SCALE = 1

def branch_y_positions(n: int) -> List[float]:

    """
    Evenly spaced y positions for n branches, symmetric around 0.
    """
    if n <= 1:
        return [0.0]
    # Spread between +1 and -1
    top = 1.0
    bottom = -1.0
    step = (top - bottom) / (n - 1)
    return [top - i * step for i in range(n)]

def draw_rbd_recursive(root_block: Dict[str, Any],
                       comp_data: Dict[str, Dict[str, float]],
                       title: str,
                       no_bundle) -> None:
    G = nx.DiGraph()
    pos: Dict[str, Tuple[float, float]] = {}
    labels: Dict[str, str] = {}

    uid = {"n": 0}

    def new_id(prefix: str = "N") -> str:
        uid["n"] += 1
        return f"{prefix}{uid['n']}"

    def add_node(nid: str, label: str, x: float, y: float):
        G.add_node(nid)
        pos[nid] = (x, y)
        labels[nid] = label
```

```
def add_edge(a: str, b: str):
    G.add_edge(a, b)


def node_label_for_component(name: str) -> str:
    A = get_component_A(name, comp_data)
    R = get_component_R(name, comp_data, MISSION_TIME_HR)
    return f"{name}\nA={fmt15(A)}\nR={fmt15(R)}"


def draw_node(node: Node, x0: float, y0: float) -> Tuple[str, str, float]:

    # Component
    if isinstance(node, str):
        nid = new_id("C_")
        add_node(nid, node_label_for_component(node), x0, y0)
        return nid, nid, x0
    # Bundle (collapsed series node)
    if is_bundle(node):
        names = node["names"]
        Aeq = 1.0
        for nm in names:
            Aeq *= get_component_A(nm, comp_data)

        nid = new_id("B_")

        # Label: join names (but avoid extreme label length)
        joined = " + ".join(names)
        if len(joined) > 60:
            joined = joined[:57] + "..."

        add_node(nid, f"{joined}\nA={fmt15(Aeq)}", x0, y0)
        return nid, nid, x0


    # Block
    if not isinstance(node, dict):
        raise TypeError(f"Invalid node type in draw: {type(node)} {repr(node)}")

    btype = node.get("type")
    bid = node.get("id", btype)
```

```
    # SERIES
    if btype == "series":
        items = node.get("items", None)
        if items is None:
            items = node.get("components", [])
        items = compress_consecutive_strings(items, no_bundle)


        if not isinstance(items, list):
            raise TypeError("series.items must be a list")

        entry = None
        prev_exit = None
        xr = x0

        for it in items:
            en, ex, xr_it = draw_node(it, xr, y0)
            if entry is None:
                entry = en
            if prev_exit is not None:
                add_edge(prev_exit, en)
            prev_exit = ex
            xr = xr_it + 1

        if entry is None or prev_exit is None:
            # empty series
            dummy = new_id("EMPTY_SER_")
            add_node(dummy, f"{bid}\n(empty series)", x0, y0)
            return dummy, dummy, x0

        return entry, prev_exit, xr - 1

    # PARALLEL
    if btype == "parallel":
        branches = node.get("branches", None)
        if branches is None:
            comps = node.get("components", [])
            branches = [[c] for c in comps]

        branches = [compress_consecutive_strings(b, no_bundle) for b in branches]
```

```
        if not isinstance(branches, list) or any(not isinstance(b, list) for b in branches):
            raise TypeError("parallel.branches must be a list of lists")

        split = new_id("SPLIT_")
        merge = new_id("MERGE_")
        add_node(split, f"{bid}\nSplit", x0, y0)

        ys = branch_y_positions(len(branches))
        branch_exits: List[str] = []
        xr_max = x0

        for bi, branch in enumerate(branches):
            yb = y0 + BRANCH_Y_SCALE * ys[bi]
            xr = x0 + 1
            prev_exit = split
            first_entry = None

            for it in branch:
                en, ex, xr_it = draw_node(it, xr, yb)
                if first_entry is None:
                    first_entry = en
                    add_edge(split, first_entry)
                else:
                    add_edge(prev_exit, en)
                prev_exit = ex
                xr = xr_it + 1

            # If branch is empty, connect split directly to merge later
            if first_entry is None:
                branch_exits.append(split)
            else:
                branch_exits.append(prev_exit)

            xr_max = max(xr_max, xr - 1)

        add_node(merge, f"{bid}\nMerge\nparallel(1oo{len(branches)})", xr_max + 1, y0)
        for ex in branch_exits:
            add_edge(ex, merge)

        return split, merge, xr_max + 1
```

```
        raise ValueError(f"Unsupported block type in draw: {btype}")

    # Build full diagram: START -> root -> END
    start = "START"
    end = "END"
    add_node(start, "START", 0, 0)

    root_entry, root_exit, xr = draw_node(root_block, 1, 0)
    add_edge(start, root_entry)

    add_node(end, "END", xr + 2, 0)
    add_edge(root_exit, end)

#plot proerties
    plt.figure(figsize=(14, 7))
    nx.draw(
        G,
        pos,
        with_labels=False,
        arrows=True,
        node_color="skyblue",
        node_size=900,
        linewidths=0.5
    )
    for nid, (xn, yn) in pos.items():
        plt.text(xn, yn + 0.12, labels[nid], ha="center", va="bottom", fontsize=9)

    plt.title(title)
    plt.axis("off")
    plt.tight_layout()
    plt.show()


# =========================
# MAIN
# =========================

def main():
    topology = load_topology(TOPOLOGY_PATH)
    comp_data = load_components(COMPONENTS_PATH)
    NO_BUNDLE = set(topology.get("no_bundle", []))
```

```
    if "root" not in topology:
        raise KeyError(
            "Your topology.json must contain a top-level key 'root' for the nested schema.\n"
            "Example:\n"
            '{\n  "system_name":"...",\n  "root": { "id":"...", "type":"parallel", ... }\n}\n'
        )

    root = topology["root"]

    A_sys = compute_block_availability(root, comp_data)
    U_sys = 1.0 - A_sys
    R_sys = compute_block_reliability(root, comp_data, MISSION_TIME_HR)
    F_sys = 1.0 - R_sys  # probability of at least one failure within mission time


    print(f"System Availability A_sys   = {fmt15(A_sys)}")
    print(f"System Unavailability U_sys = {fmt15(U_sys)}")
    print(f"System Reliability R_sys(t) = {fmt15(R_sys)}  (t = {MISSION_TIME_YEARS} years)")
    print(f"System Failure Prob F_sys   = {fmt15(F_sys)}  (within mission time)")

    draw_rbd_recursive(
        root_block=root,
        comp_data=comp_data,
        title=f"{topology.get('system_name','System')} — Nested RBD\nA_sys={fmt15(A_sys)} | U_sys={fmt15(U_sys)}",
        no_bundle=NO_BUNDLE
    )


if __name__ == "__main__":
    main()
```

B.2 AC Upstream Topology

The AC architecture topology is defined in JSON format.

The structure follows a hierarchical nested schema composed of:

- "series" blocks

- "parallel" blocks
- Component identifiers (strings)

The key element of the file is the "root" block, which represents the full system from upstream MV/LV interface to the PDU bus.

Parallel branches represent redundant paths (1-out-of-n configuration), while series blocks represent mandatory sequential components.

```
{"system_name": "AC",
"no_bundle": ["inverter"],

"root": {"id": "PDU_bus","type": "series","items": [

"Upstream",
{
 "id": "UPS_Bypass","type": "parallel","branches": [
 [
  {"id": "UPS_branch","type": "series","items": [

    "till_MV-LV", "MVLV_TRANSF", "MVLV_transf_bus",

   {"id": "Bypass_connection","type": "parallel","branches": [
[
     {"id": "UPS_path", "type": "series", "items":[

         "MVLV_transf_bus_CB3", "CAVO_MVLV_transf_bus_TO_1S-PA-UPS1",
        {"id": "building_UPS", "type": "parallel", "branches":[
          ["rectifier"], ["battery"]]}
, "inverter", "CABLE_4", "bypasss_CB"]}

]
,
                ["MVLV_transf_bus_CB4",        "CAVO_MVLV_transf_bus_TO_1S-PA-UDP1",
"CB_6"]
              ]
            }
          ]
        },
"CB"
      ],
```

["till_MV-LV_ext", "EXT_TRANSF", "ext_trans_BUS", "ext_trans_BUS_CB", "CAVO_ext_trans_BUS_TO_bypass_BUS", "bypass_BUS", "bypass_BUS_CB1", "CABLE_2", "CB_2"]
]
},

"UDP_bus", "UDP_bus_CB", "CABLE_7", "UPS_in_CB", "ISOLATIO_TRANS", "UPS_out_CB", "PDU_bus"
]
}
}

B.3 DC Upstream Topology

{"system_name": "DC",
"no_bundle": [],
"root": {"id": "PDU_bus","type": "series","items": [

"Upstream",
{
"id": "UPS_Bypass","type": "parallel","branches": [
[
{"id": "UPS_branch","type": "series","items": [
"till_MV-LV", "MVLV_TRANSF", "rectifier", "MVLV_transf_bus",

{"id": "Bypath_connection","type": "parallel","branches": [
[
{"id": "UPS_path", "type": "series", "items":[

"MVLV_transf_bus_CB3", "CAVO_MVLV_transf_bus_TO_1S-PA-UPS1",
{"id": "building_UPS", "type": "parallel", "branches":[
["one"], ["battery"]]}
, "CABLE_4", "bypasss_CB"]}

]
,
["MVLV_transf_bus_CB4", "CAVO_MVLV_transf_bus_TO_1S-PA-UDP1", "CB_6"]
]
}
]
},
"CB"

```
      ],
      ["till_MV-LV_ext", "EXT_TRANSF", "rectifier", "ext_trans_BUS",
"ext_trans_BUS_CB", "CAVO_ext_trans_BUS_TO_bypass_BUS", "bypass_BUS",
"bypass_BUS_CB1", "CABLE_2", "CB_2"]
    ]
  },

"UDP_bus", "UDP_bus_CB", "CABLE_7", "UPS_in_CB", "PDU_bus"
]
  }
}
```

B.4 Downstream Topology

```
{"system_name": "Downstream",

"root":
{"id": "RPP_path","type": "series","items": [
 "PDU_bus_CB01", "CAVO_PDU_bus_TO_PAN1", "PDU_bus_PANEL1"]}
}
```

B.5 AC Components

The component database contains MTBF and MTTR values derived from IEEE Std. 493 (Gold Book).

For confidentiality reasons, component identifiers have been anonymized. The reliability parameters remain unchanged.

The CSV file contains the following fields:

- component
- mtbf_hr
- mttr_hr

component	mtbf_hr	mttr_hr
Upstream	1E+09	0
till_MV-LV_bus	1E+09	0
till_MV-LV_ext	1E+09	0
EXT_TRANSF	14432242	0
ext_trans_BUS	9461587	0

ext_trans_BUS_CB	77665552	18.67
CAVO_ext_trans_BUS_TO_bypass_BUS	4230969	8
bypass_BUS	14192381	0
bypass_BUS_CB1	77665552	18.67
CABLE_2	4230969	8
CB_2	77665552	18.67
MVLV_TRANSF	14432242	0
MVLV_transf_bus	18923174	0
MVLV_transf_bus_CB3	55821363	0
CAVO_MVLV_transf_bus_TO_1S-PA-UPS1	6346453	8
battery	1173590	32.13
inverter	1817016	26
rectifier	1960032	16
CABLE_4	4230969	8
bypasss_CB	55821363	0
MVLV_transf_bus_CB4	77665552	18.67
CAVO_MVLV_transf_bus_TO_1S-PA-UDP1	4230969	8
CB_6	77665552	18.67
UDP_bus	23653968	0
UDP_bus_CB	55821363	0
CABLE_7	42309688	8
UPS_in_CB	55821363	0
ISOLATIO_TRANS	3087253	21.26
UPS_out_CB	55821363	0
PDU_bus	33115555	0
PDU_bus_CB01	55821363	0
CAVO_PDU_bus_TO_PAN1	84619377	8
PDU_bus_PANEL1	42577142	0

B.6 DC components

component	mtbf_hr	mttr_hr
Upstream	1E+09	0
till_MV-LV	1E+09	0
till_MV-LV_ext	1E+09	0
one	1.00E+11	0
EXT_TRANSF	14432242	0
ext_trans_BUS	9461587	0
ext_trans_BUS_CB	13840094	0
CAVO_ext_trans_BUS_TO_bypass_BUS	394895	2
bypass_BUS	14192381	0
bypass_BUS_CB1	13840094	0
CABLE_2	394895	2
CB_2	13840094	0
MVLV_TRANSF	14432242	0
MVLV_transf_bus	18923174	0
MVLV_transf_bus_CB3	13840094	0
CAVO_MVLV_transf_bus_TO_1S-PA-UPS1	592342.5	2
battery	4.29E+09	32.13
CABLE_4	394895	2
bypasss_CB	13840094	0
MVLV_transf_bus_CB4	13840094	0
CAVO_MVLV_transf_bus_TO_1S-PA-UDP1	394895	2
CB_6	13840094	0
1S-PA-UDP1_CB_Q4	13840094	0
UDP_bus	23653968	0
UDP_bus_CB	13840094	0
CABLE_7	3948950	2
UPS_in_CB	13840094	0
PDU_bus	33115555	0
PDU_bus_CB01	13840094	0
CAVO_PDU_bus_TO_PAN1	7897900	2
PDU_bus_PANEL1	42577142	0
rectifier	1960032	16

List of Figures

List of Tables

List of symbols

Variable	Description	unit
A	Availability	-
AC	Alternating Current	-
AI	Artificial Intelligence	-
C	Cable Cost	€
Cap-Ex	Capital Expenditure	-
CSA	Cross Sectional Area	mm^2
DC	Direct Current	-
E	Energy	kWh
EEA	European Environment Agency	-
EV	Electric Vehicle	-
I	Current	A
IT	Information Technology	-
J	Current Density	A/mm^2
k-oo-n	K out of n	-
L	Cable Length	m
LB	Load Bank	-
LV	Low Voltage	-
m	Copper mass per meter	kg/m
M	Copper Mass	kg
MTBF	Mean Time Between Failure	h
MTTR	Mean Time to Repair	h
MV	Medium Voltage	-
N	Neutral	-
Op-Ex	Operational Expenditure	-
P	Power	kW
PDU	Power Distribution Unit	-
PE	Protective Earth	-
pf	Power Factor	-
PUE	Power Usage Effectiveness	-
QoS	Quality of Service	-

r	Battery Recharge Rate	-
R	Resistance	Ω
R(t)	Reliability	-
RBD	Reliability Block Diagram	-
RMS	Root Mean Square	-
RPP	Remote Power Panel	-
SLD	Single Line Diagram	-
UDP	UPS Distribution Panel	-
UPS	Uninterruptible Power Supply	-
V	Voltage	V
VD	Voltage Drop Percentage	-
Vol	Copper Volume	m^3
WHR	Waste Heat Recovery	-
X	Inductive reactance	Ω
ΔV	Voltage Drop	V

Acknowledgments

I would like to express my sincere gratitude to my supervisor, Prof. Morris Brenna, for his guidance, valuable feedback, and academic support throughout the development of this thesis. His expertise and constructive insights were fundamental in shaping both the technical depth and the overall structure of this work.

I would also like to thank Osama Elhassan for his support and practical guidance from an industrial perspective. His availability, technical discussions, and professional insight significantly contributed to the realism and applicability of the analysis presented in this thesis.

I am sincerely grateful to Gloria Monteleone for facilitating the connection between Politecnico di Milano and STACK Infrastructure and for her support in enabling this collaboration. I would also like to thank Francesco Stroppa from STACK Infrastructure HR for his coordination and communication with the university, which helped make this opportunity possible. Furthermore, I would like to express my appreciation for STACK Infrastructure for providing the opportunity to carry out this thesis within a professional and technically stimulating environment. My thanks also extend to all members of the STACK team, who were consistently kind, supportive, and willing to share their knowledge throughout this experience.

Finally, I would like to acknowledge all those who indirectly supported this work through discussions, feedback, and encouragement during my studies.